Intercomparison of meteorological observation systems on the R/V *Kilo Moana* and WHOTS buoys

2009 WHOTS-6 Field Program.

July 9 – July 17, 2009

Ludovic Bariteau[1], Jeff Hare[1], C. W. Fairall[2], Sergio Pezoa[2], Dan Wolfe[2], Nan Galbraith[3], Frank Bradley[4], Kelan Huang[3], Frank Bahr [3], Sean P. Whelan[3], Al Plueddemann[3], Roger Lukas[5], Paul Lethaby[5], Anita D. Rapp[6]

1 Cooperative Institute for Research in Environmental Sciences (CIRES)

2 NOAA Earth System Research Laboratory (ESRL), Physical Sciences Division

3 Woods Hole Oceanographic Institution (WHOI)

4 Commonwealth Scientific and Industrial Research Organization (CISRO), Australia

5 University of Hawaii (UH)

6 Texas A&M University

November 26, 2010

Table of contents

List of Figures

List of Tables

1) Introduction and Goals

The R/V (Research Vessel) *Kilo Moana* is a twin hull oceanographic research ship (Figure 1) designed for oceanographic research in coastal seas and deep ocean areas. The ship is operated by the School of Ocean and Earth Science and Technology at the University of Hawaii. Since 2007, part of the ship's annual schedule includes servicing surface moorings as part of the Woods Hole Oceanographic Institute (WHOI) Hawaii Ocean Time-series Station (WHOTS) project.

As part of this effort, the Earth System Research Laboratory (ESRL) Physical Science Division (PSD) Air-Sea Interaction group participated in the WHOTS-6 cruise (Whelan et al., 2010), providing a portable flux calibration facility to provide high quality observations for comparison with the WHOTS buoys and for calibration and intercomparison of the Kilo Moana's suite of meteorological instruments.

In this report, we describe the meteorological sensor comparisons between the ship, the buoys, and the NOAA/ESRL/PSD system. In Section 1, the different suites of instruments used in this comparison are described. Section 2 shows the analysis procedures used for the comparison. Results and discussion are provided in Section 3. Finally, conclusions are given in Section 4.

Figure 1. Aerial view of the R/V Kilo Moana.

2) Instrumentation description

a) Description of the NOAA/ESRL/PSD system

A 10-m tower was set up on the 01 deck of the portside bow of the ship (Figure 2). The fast turbulence system installed on the bow tower is composed of a Gill-Solent sonic anemometer, a Li-Cor LI-7500 fast CO_2/hygrometer, and a Systron-Donner motion-pak. A Vaisala mean temperature/humidity (T/RH) sensor in an aspirator and an optical rain gauge (ORG) were also mounted on the bow tower. To complete the PSD air-sea flux system, pyranometers and pyrgeometers (Eppley and Kipp&Zonen) were mounted on top of pole on the 03 deck (Figure 3). Finally, a near surface sea surface temperature (SST) sensor ('sea snake') consisting of a floating thermistor was deployed from the portside pontoon. A second sonic anemometer was also deployed on the bridge mast (Figure 6).

Figure 2. Left: Flux tower deployed at the bow of the portside pontoon. The sea surface thermistor, i.e. 'sea snake', can be seen on the inboard side of the pontoon (red arrow). Right: Close-up view of the tower and its instruments

Figure 3. View of the tower and the radiometers from the 3rd deck (red arrows).

Slow mean data (T/RH, radiometers, etc) are digitized on two Campbell dataloggers and transmitted via wireless modem in 1-minute averages. Inside the operation van, deployed further aft on the portside pontoon of the 01 deck (see Figure 4), a central data acquisition computer logs continuously all sources of data via RS-232 digital transmission and wireless radio modem network. The operation van also contains a W-band Doppler cloud radar (Moran K. et al., 2010). Table 1.1 shows sampling rates and deployment heights of the PSD sensors.

Figure 4. View of the operation van deployed on 01 deck of the Kilo Moana. The bow tower can be seen on the background (red arrow**).**

Sensor	Sampling rate	Height (m)
Bow sonic	10 Hz	17.4
Bridge sonic	10 Hz	21.3
Motion Pack	10 Hz	17.2
ORG	0.1Hz, averaged to 1 sample/min	15.7
T/RH	0.1Hz, averaged to 1 sample/min	14.7
Licor (CO2&H2O)	10 Hz	16.6
Radiometers	0.1Hz, averaged to 1 sample/min	14.4
Barometer	0.1Hz, averaged to 1 sample/min	13.3
SST	0.1Hz, averaged to 1 sample/min	-0.05 to -0.10

Table 1. PSD sensor heights and sampling rates.

b) Description of KM system

Most of the ship's meteorological instruments are located on a mast situated about 6m above the 04 deck (Figure 5). This includes two RM Young anemometers (port and starboard), a Rotronics air temperature/humidity unit (T/RH), an RM Young Resistive Temperature Device (RTD), one each of siphon and optical raingauges, and a pair of Eppley longwave (PIR) and shortwave (PSP) radiometers. See Appendix A (Figures A1 and A2) for a close-up view of the suite of instruments at the top of the ship's mast.

Figure 5. Instrument mast on top of the wheelhouse of the Kilo Moana.

The ship's barometer is located in an aft laboratory near the working deck (see Figure A3). The Inertial Measurement Unit (IMU) of the Position and Orientation System for Marine

Vessels (POSMV) system is located in the sonar room on the port pontoon. The ship's thermosalinograph (UTHSL) is mounted in a laboratory well forward in the port hull. Signals from these sensors are recorded and made available continuously on the ship's network. The instrument heights and available data rate are described in Table 1.2.

Sensor	Available data rate	Height (m)
Anemometer	0.5Hz	21.4
ORG	1Hz	20.7
T/RH	1Hz	19.7
RTD	1Hz	20.1
Radiometers	1Hz	21.2
Barometer	1Hz	4.8
SST (uthsl)	1Hz	-7.0
POSMV	1Hz	--

Table 2. KM sensor heights and available data rates.

c) Description of the AUTOimet system

An AutoIMET (AI) system from WHOI was also installed alongside the ship's instruments on the mast above the bridge. It included a pair of radiometers (Eppley PIR/PSP), a T/RH unit (naturally ventilated shield), a barometer and a siphon raingauge (see figure A2 for a close-up view of these instruments). The AI wind sensor was set up below the mast on the forward rail of the 04 deck (Figure 6).

Figure 6. Side view of the AI wind sensor with the ship's mast in the background. The second PSD sonic can be seen on a ~1m boom setup on top of the mast.

Data from the AutoIMET are recorded once per minute in a logger situated on the tower and were made available continuously on the ship's network at two-minute data rate. A description of the AI instrument heights and available data rate is given in Table 1.3.

Sensor	Available rate	Height (m)
Anemometer	1-minute data	17
Siphon rain	1-minute data	21
T/RH	1-minute data	21.2
PIR/PSP	1-minute data	21.6
Barometer	1-minute data	20.6

Table 3. AutoIMET sensor heights and available data rates.

d) WHOTS buoys IMET sensors

On the WHOTS buoys, the identical meteorological instruments as the AutoIMET are used with different packaging and are typically deployed in pairs. The variables of interest for this report are: short wave and long wave radiation (Eppley), air temperature and specific humidity, barometric pressure, wind speed and direction, and sea surface temperature. The data are logged as one minute averages and are available once the buoy is recovered. Hourly averaged data are transmitted via Argos satellite telemetry and are available in real time. Details of the WHOTS-5 and WHOTS-6 buoy (see Figure 7) data rate and instrument heights are given in Tables 1.4 and 1.5.

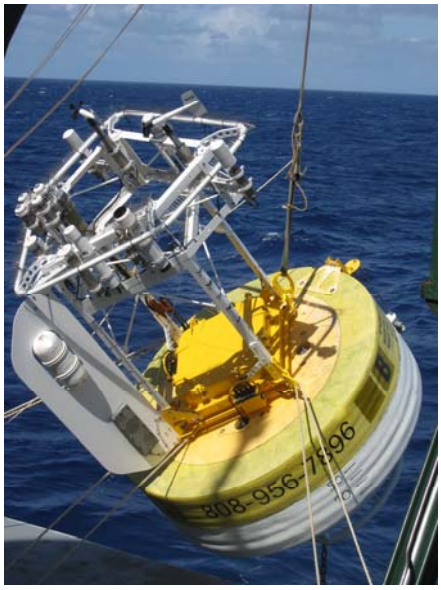

Figure 7. View of WHOTS-6 buoy and its meteorological instruments during deployment.

Sensor	Available rate	Height (m)
Anemometer	1-min data	3.26
Siphon rain	1-min data	3.11
T/RH	1-min data	2.89
Radiometers	1-min data	3.5
Barometer	1-min data	2.98
SST	1-min data	-0.91

Table 4. WHOTS-5 buoy sensor heights and available data rates.

Parameter	Available rate	Height (m)
Anemometer	1-hour data	3.32
Siphon rain	1-hour data	3.12
T/RH	1-hour data	2.92
Radiometers	1-hour data	3.4
Barometer	1-hour data	3.01
SST	1-hour data	-0.88

Table 5. WHOTS-6 buoy sensor heights and available data rates.

3) Method

The dual purpose of the WHOTS-6 cruise was to deploy one surface mooring (WHOTS-6) and to recover another (WHOTS-5). The R/V *Kilo Moana* departed from the UH Marine Center at Sand Island on 9 July 2009 and steamed to the WHOTS site near 22º 45' N, 158º 00' W to first deploy the WHOTS-6 mooring (Figure 8). Afterward the ship maintained position about 0.2 nm downwind of this mooring for an intercomparison period beginning at about 0500 GMT on 11-July (Day 192) until 1000 GMT on 13-July (Day 194). Then the *Kilo Moana* moved about 0.2 nm downwind of the WHOTS-5 mooring to perform another intercomparison from 1145 GMT on 13-July (Day 194) to 1500 GMT on 15-July (Day 196). After that, the WHOTS-5 buoy was recovered, and the *Kilo Moana* returned to the UH Marine center on July 17, 2009.

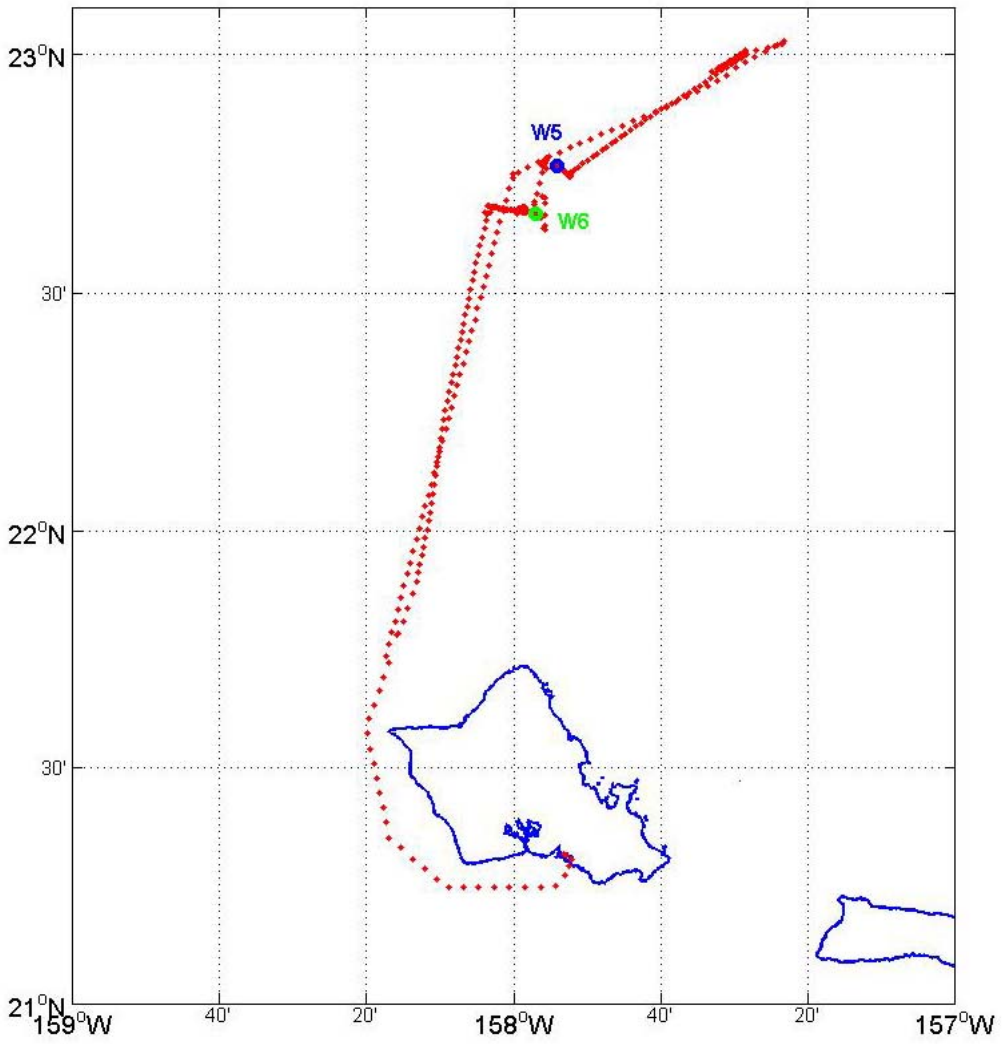

Figure 8. Cruise track of the R/V *Kilo Moana* during WHOTS-6 cruise

The 5-min average time series of true wind speed, true wind direction (relative to North), air temperature (blue), sea surface temperature (red), incident shortwave (blue) and longwave (red), relative humidity and atmospheric pressure are shown for July 9th to July 16th (Day 190-197) in Figure 9. On this plot, we can see the water temperature is relatively constant around 25.5°C, while the air temperature is slightly lower at 24.6°C. The winds were easterly with a speed averaging about 8 m.s^{-1}.

The resulting bulk air-sea fluxes for the same dates are illustrated in Figure 10. Momentum, sensible and latent heat fluxes are computed using the COARE bulk algorithm version 3.0 (Fairall et al., 2003). The mean net surface heat gain during the studied period was about 89 Wm^{-2} (Table 1.6)

Variable	Mean	Max	Min	Standard deviation
WS ($m.s^{-1}$)	7.83	12.76	3.54	1.12
WD (deg)	80.70	130.42	42.06	10.53
Tair (C)	24.61	27.57	22.24	0.57
SST (C)	25.52	26.71	24.75	0.17
RH (%)	75.49	88.75	54.04	4.10
Atm Pressure (mb)	1016.55	1018.31	1014.20	0.85
Stress ($N. m^{-2}$)	0.08	0.27	0.02	0.03
Hnet ($W. m^{-2}$)	89.12	976.08	-325.25	359.93
Rs ($W. m^{-2}$)	293.63	1145.04	-0.30	357.33
Rnl ($W. m^{-2}$)	-59.66	-11.68	-78.65	13.4
Hsb ($W. m^{-2}$)	6.26	35.10	-12.53	4.65
Hlb ($W. m^{-2}$)	133.65	238.94	84.40	19.87

Table 6. Mean conditions during WHOTS-6 cruise.

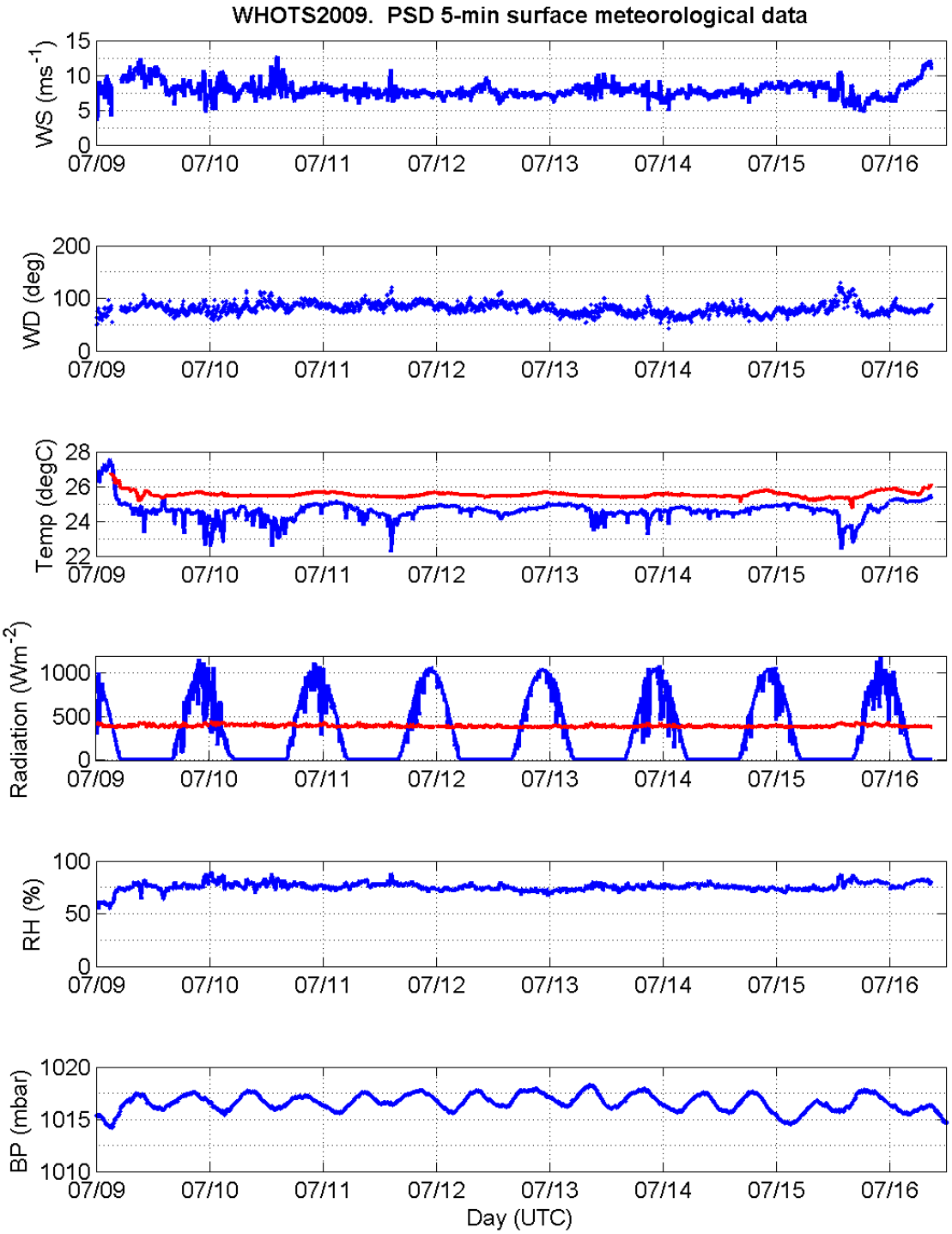

Figure 9. Meteorological conditions during WHOTS-6 from July 9th to July 16th, 2009. From the top, the panels show the wind speed ($m.s^{-1}$), the wind direction in degrees relative to North, the air temperature in blue and SST in red (°C), the incident shortwave (blue) and longwave (red) radiations ($W.m^{-2}$), the relative humidity (%) and the barometric pressure (mb).

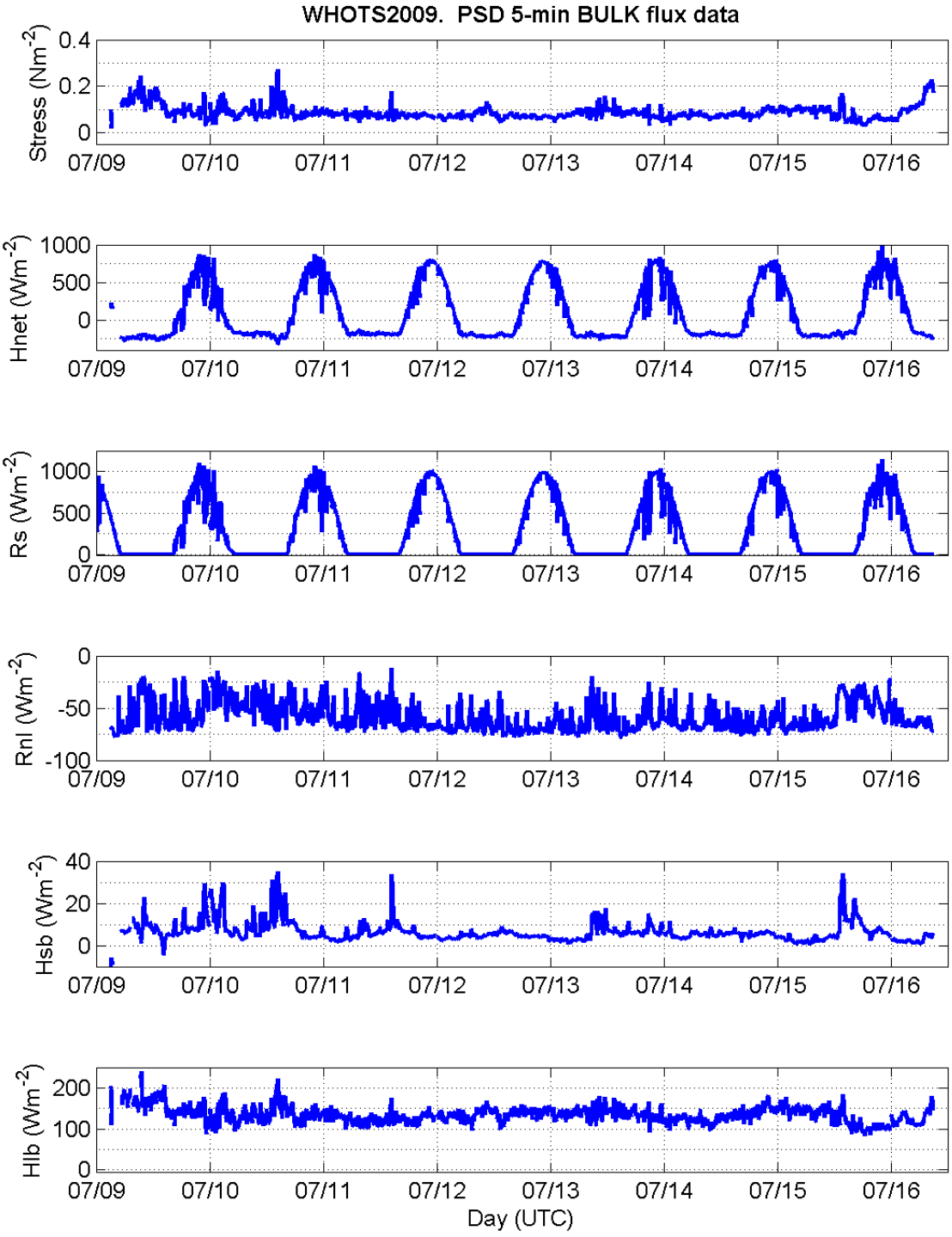

Figure 10. Bulk surface fluxes during WHOTS-6 from July 9th to July 16th, 2009. From the top, the panels show the longitudinal component of the wind stress ($N.m^{-2}$), the net heat flux ($W.m^{-2}$), the solar flux ($W.m^{-2}$), the net longwave radiation flux ($W.\ m^{-2}$), the sensible heat flux ($W.\ m^{-2}$) and the latent heat flux ($W.\ m^{-2}$).

During these 8 days at sea, two strategies were used to compare the different sets of observations between the NOAA/ESRL/PSD, the ship, the AutoIMET and the two buoy systems. The first strategy was to compare the PSD, AutoIMET and ship's instruments for the entire cruise. Due to the difference in sensor heights and sampling strategy, the following steps were employed:

- meteorological variables were adjusted to a reference height of 10m by using the COARE3.0 bulk flux algorithm (Fairall et al., 2003). The variables adjusted at 10m are wind speed, air temperature, and relative humidity
- the PSD instruments were used as the reference for the comparisons
- standard meteorological wind direction was adopted for all of observations
- due to the disparity of sampling strategies, all the data were averaged to one-minute to match the sampling rate of the AutoIMET system

The second strategy was to compare the PSD, AutoIMET, ship instruments with the two buoys during the intercomparison days mentioned previously. Similarly, the following steps were taken:

- air temperature and relative humidity were adjusted to the buoy height of 2.89m, while the wind variable was adjusted to a height of 3.26m (see Table 5-2 in Whelan et al., 2010)
- standard meteorological wind direction was adopted for all the different sets of observations.
- for the comparison with WHOTS-5 and WHOTS-6 buoys, all the data were averaged to one-minute.
- the data from the WHOTS-5 buoy were edited using one ASIMET logger,

or a composite that uses sections of data from each logger. With regard to the WHOTS-6 buoy data (recovered July 2010), the data were unedited and both data loggers were used in the comparison. The buoy data were used as references in this comparison.

In what follows, KM refers to *Kilo Moana*, AI to the AutoIMET system and PSD to the NOAA/ESRL/PSD system. W5 refers to WHOTS-5 edited buoy data, and W6_7 and W6_19 refer to the loggers 7 and 19 on WHOTS-6 buoy. Table 1.7 summaries the sensor acronyms that will be used in the next sections. For instance, the PSD pyranometers and pyrgeometers

(Eppley and Kizz&Zonen) will be referred as ‘PSD Eppley’ and ‘PSD K&Z’ respectively. The PSD sonic deployed at the bow tower will be designated by ‘PSD bow’, while ‘PSD bridge’ will refer to the sonic deployed on the bridge mast. The KM Rotronics air temperature/humidity unit and RM Young Resistive Temperature Device will be named as ‘KM rot’ and ‘KM rtd’ respectively. Finally, the two RM Young anemometers of the KM will be referred as ‘KM port’ and ‘KM stbd’ for portside and starboard location.

Parameter	**PSD**	**KM**	**AI**	**WHOTS-5 buoy**	**WHOTS-6 buoy**
Air temperature	PSD	KMrot & KMrtd	AI	W5	W6_7 & W6_19
Relative humidity	PSD	KMrot	AI	W5	W6_7 & W6_19
Sea temperature	PSD	KM	AI	W5	W6_7 & W6_19
Longwave and Shortwave radiation	PSD Eppley & PSD K&Z	KM	AI	W5	W6_7 & W6_19
Wind speed and direction	PSD bow & PSD bridge	KM port & KM stbd	AI	W5	W6_7 & W6_19

Table 7. Legend for sensors used in this report.

4) PSD, Ship and AutoIMET comparison

In this section, we compare the various instruments installed on the *Kilo Moana* with the PSD system used as reference. Air temperature, relative humidity and wind speed variables were all adjusted to a height of 10m.

a) Air temperature

Figure 11 shows the air temperature residual as a function of solar radiation. The residual is calculated as the difference between the instruments to evaluate minus the PSD instrument. Data were averaged into 25 W.m^{-2} bins of solar flux and the error bars are two standard deviation units in length. The Ship's Rotronics T/RH sensor reads about 1.1°C low when compared to the PSD unit, while the ship's RM Young device (RTD) reads about 0.5°C lower. The AI temperature sensor is in close agreement at night, but reaches about 0.2°C higher during the day.

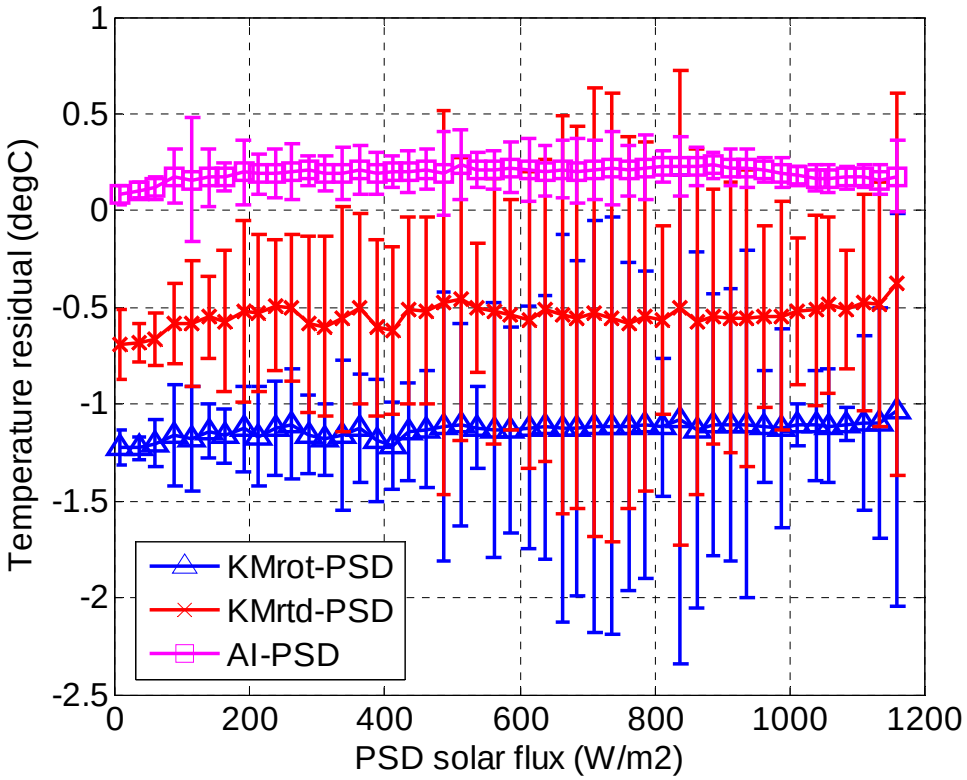

Figure 11. Dependence of air temperature residuals on solar radiation for the two ship sensors (blue and red) and the AutoIMET (magenta).

b) Relative humidity

The relative humidity residual (instrument to compare minus PSD) dependence on solar radiation shows that the PSD, KM and AI instruments are in good agreement. Figure 12 shows that the AI is reading about 1% higher than PSD, while the KM sensor is about 1% lower than PSD. The ship sensor is also more sensitive to solar heating than the AI unit (dryer air at solar peak). As with Figure 11, data were averaged into 25 $W.m^{-2}$ bins and the error bars represent two standard deviations.

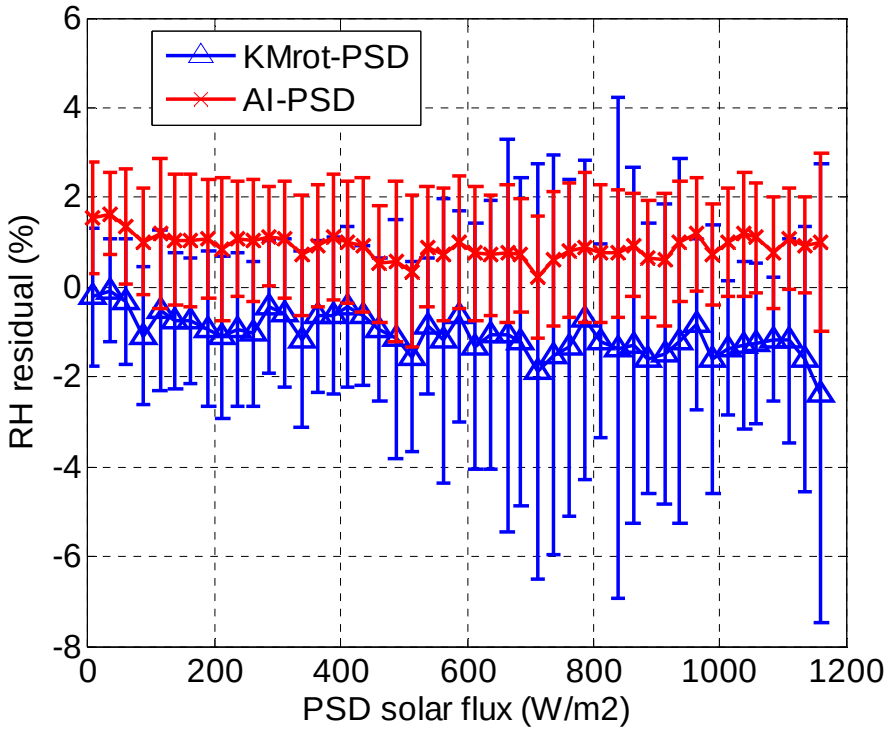

Figure 12. Relative humidity residuals as a function of solar radiation for the ship sensor (blue) and the AutoIMET (red).

c) Sea temperature

Since the AI system does not include sea surface temperature, only the ship sensor is compared to the PSD seasnake. A correction of -0.25 °C based on surface CTDs was applied to the ship's thermosalinograph temperature. Similarly, an offset correction of -0.15°C was applied to PSD temperature when compared to the other measurements. Figure 13 shows a comparison of KM and PSD sea temperature and indicates that the PSD seasnake is within 0.15°C of the thermosalinograph. The two temperatures agree well at night, but during the

day the seasnake capture the surface warming as its measurement depth is about one order of magnitude smaller than the thermosalinograph. The period 197.2-197.6 where the PSD measurement is lower during the day is when the ship was underway and the seasnake was airborne. Allowing more slack in the line got rid of the problem.

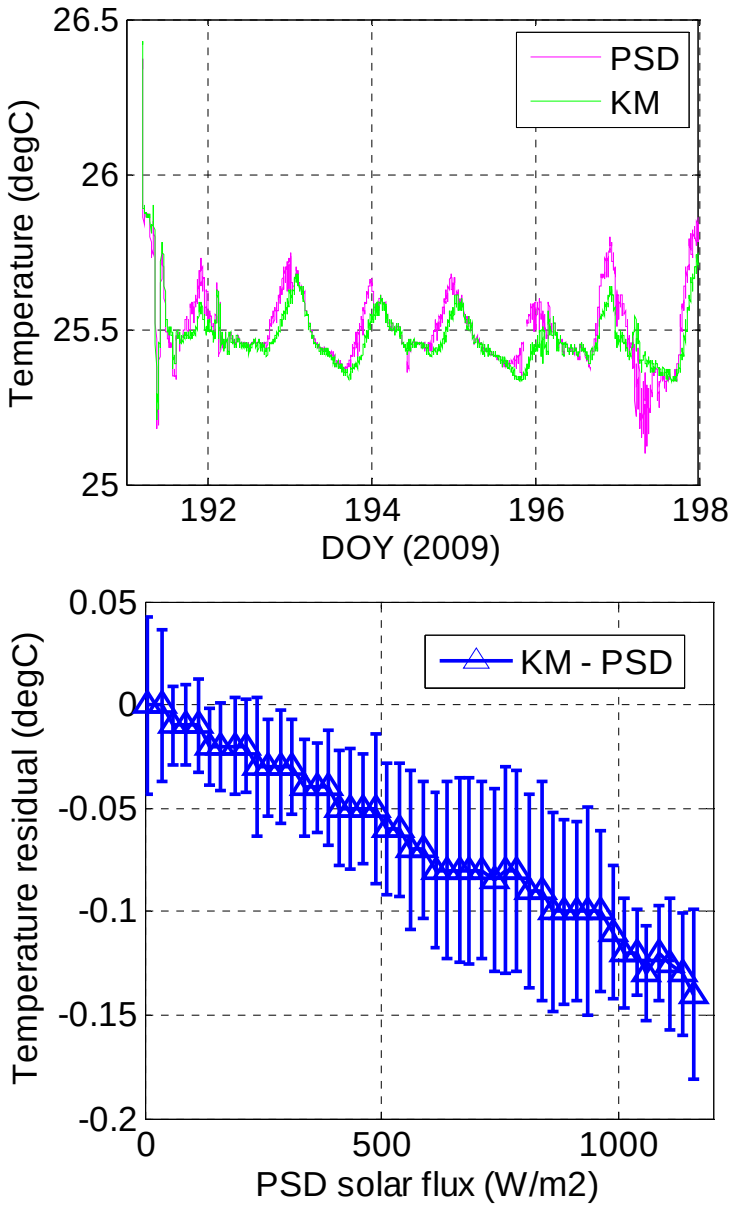

Figure 13. Comparison of seasnake with the thermosalinograph. The top panel shows a time series of the two measurements, while the lower panel shows the dependence of sea surface temperature residual as a function of solar radiation.

d) Longwave and shortwave radiation

Figure 14 shows comparison plots of the different pyrgeometers deployed on the ship. The comparisons of the two PSD units on the 3rd deck and the AI/KM units on the mast above the bridge show good correlation (right-hand side graphs). The correlation decreases slightly when comparing instruments from the bridge with instruments on the 3rd deck (left-hand side graphs). One interesting thing to notice is the difference in sensitivity between the units. To take a better look at it, we have plotted on Figure 15 the longwave radiation residual (instrument to compare minus PSD Eppley) as a function of solar radiation (data averaged into 50 $W.m^{-2}$ bins). Both the PSD Kipp&Zonen and AI pyrgeometers seem to suffer from problems of shortwave contaminations. The differences for the AI sensor range from 3 W.m-2 during the night to about 10 $W.m^{-2}$ during the day. The Kipp&Zonen differences range from about 1 $W.m^{-2}$ to 6 $W.m^{-2}$, while the KM unit is constantly about 2 $W.m^{-2}$ higher than the PSD Eppley. Although the KM unit appears to have some shortwave sensitivity problems when compare to the Eppley on Figure 14, it is not seem to be appear on Figure 15.

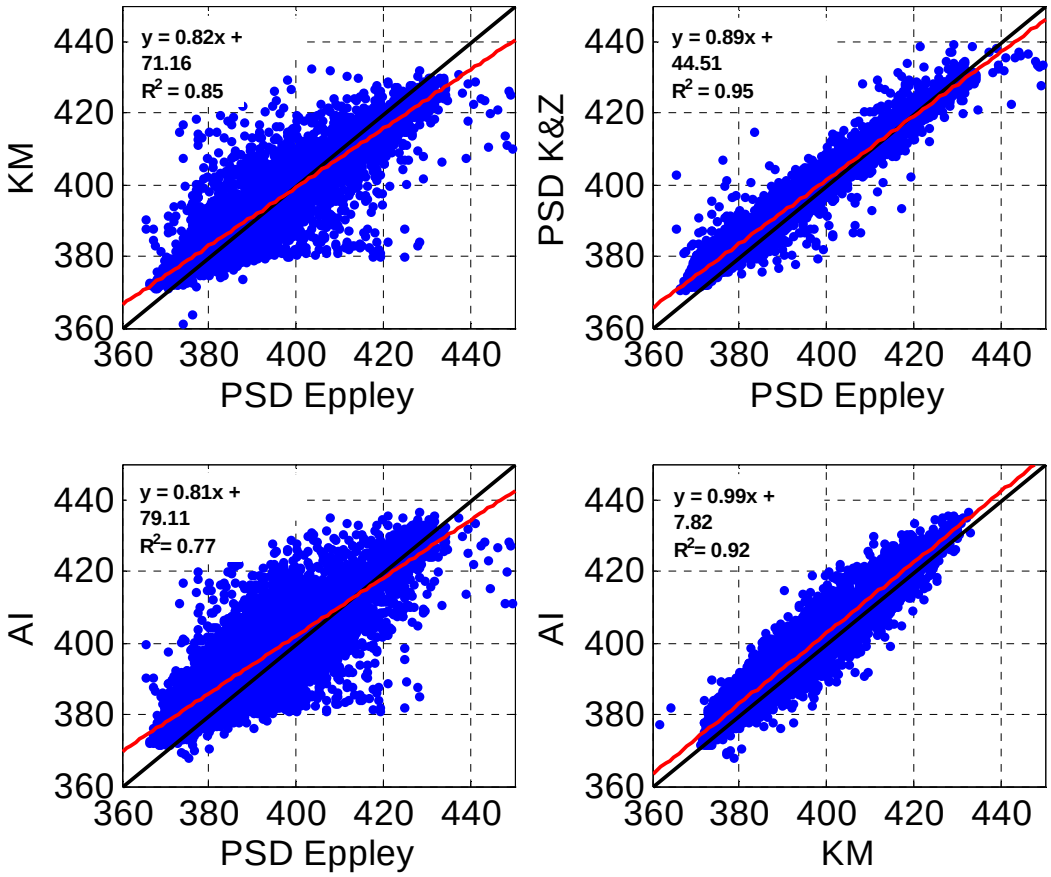

Figure 14. Comparison plots of longwave radiation for the ship, AutoIMET and PSD. The equations and squared correlation coefficients are indicated for each linear regression (red), and the black line indicates a 1:1 ratio.

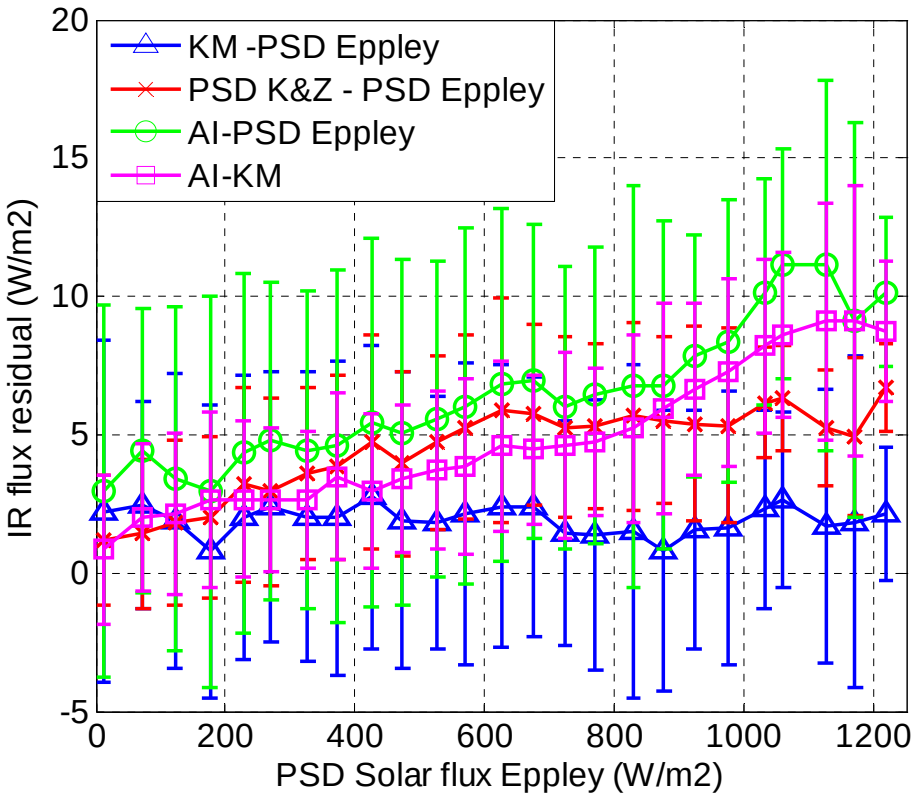

Figure 15. Dependence of longwave residuals on solar radiation for the ship (blue), the AutoIMET (green and magenta), and PSD (red)

A similar look at the pyranometer performance reveals close agreement between the different sensors. Figure 16 show that the PSD Eppley and Kipp&Zonen pyranometers track each other relatively well. However the Kipp&Zonen sensor underestimates solar radiation by about 2% (Figure 17) when compared to the Eppley. The AI pyranometer is about 7 $W.m^{-2}$ higher than the PSD Eppley in the 0 – 400 $W.m^{-2}$ range, while it underestimates solar radiation within 2% for higher range values. The KM unit is in good agreement with the PSD Eppley unit at low values, but also underestimates radiation at higher values. It is within 2% in the 0 – 200$W.m^{-2}$ and 600 – 1200 $W.m^{-2}$ ranges, while for unknown reasons is within 5% in the 200 – 600$W.m^{-2}$ region. The different locations of these instruments may explain the discrepancy.

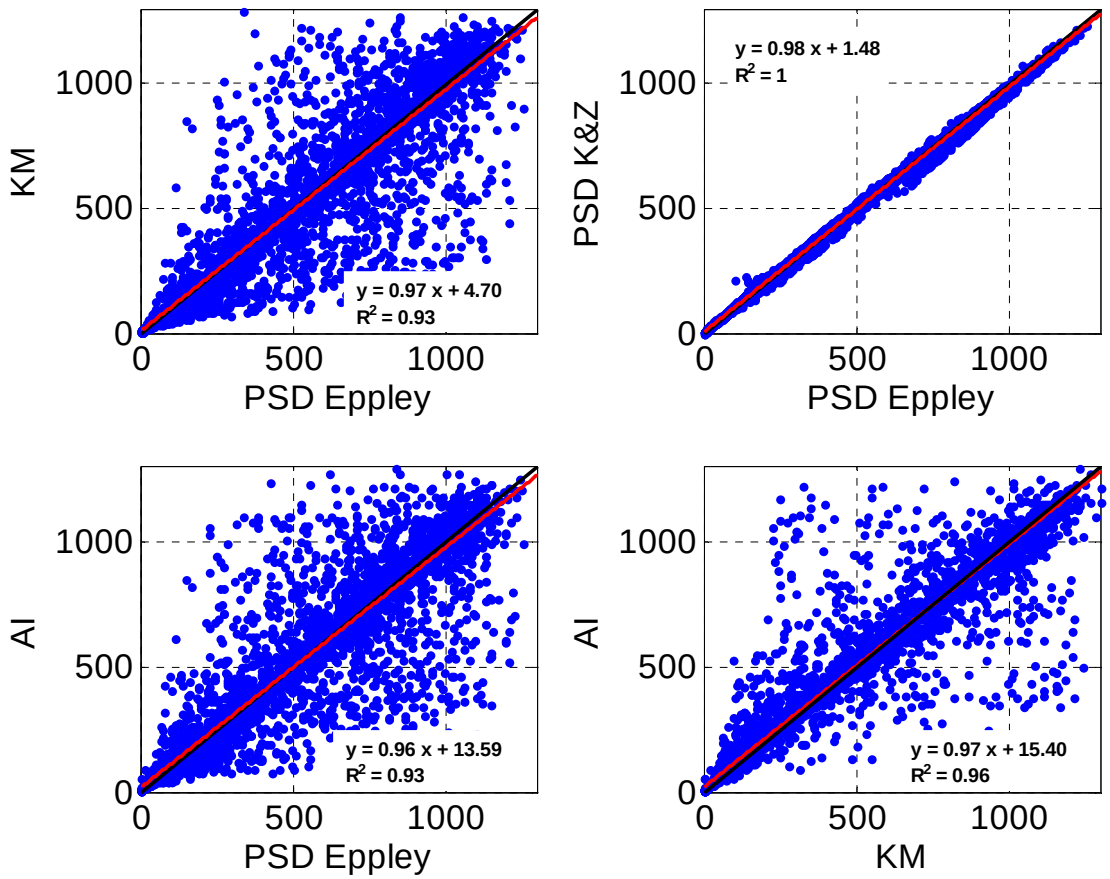

Figure 16. Comparison plots of shortwave radiation for the ship, AutoIMET and PSD. The equations and squared correlation coefficients are indicated for each linear regression (red), and the black line indicates a 1:1 ratio.

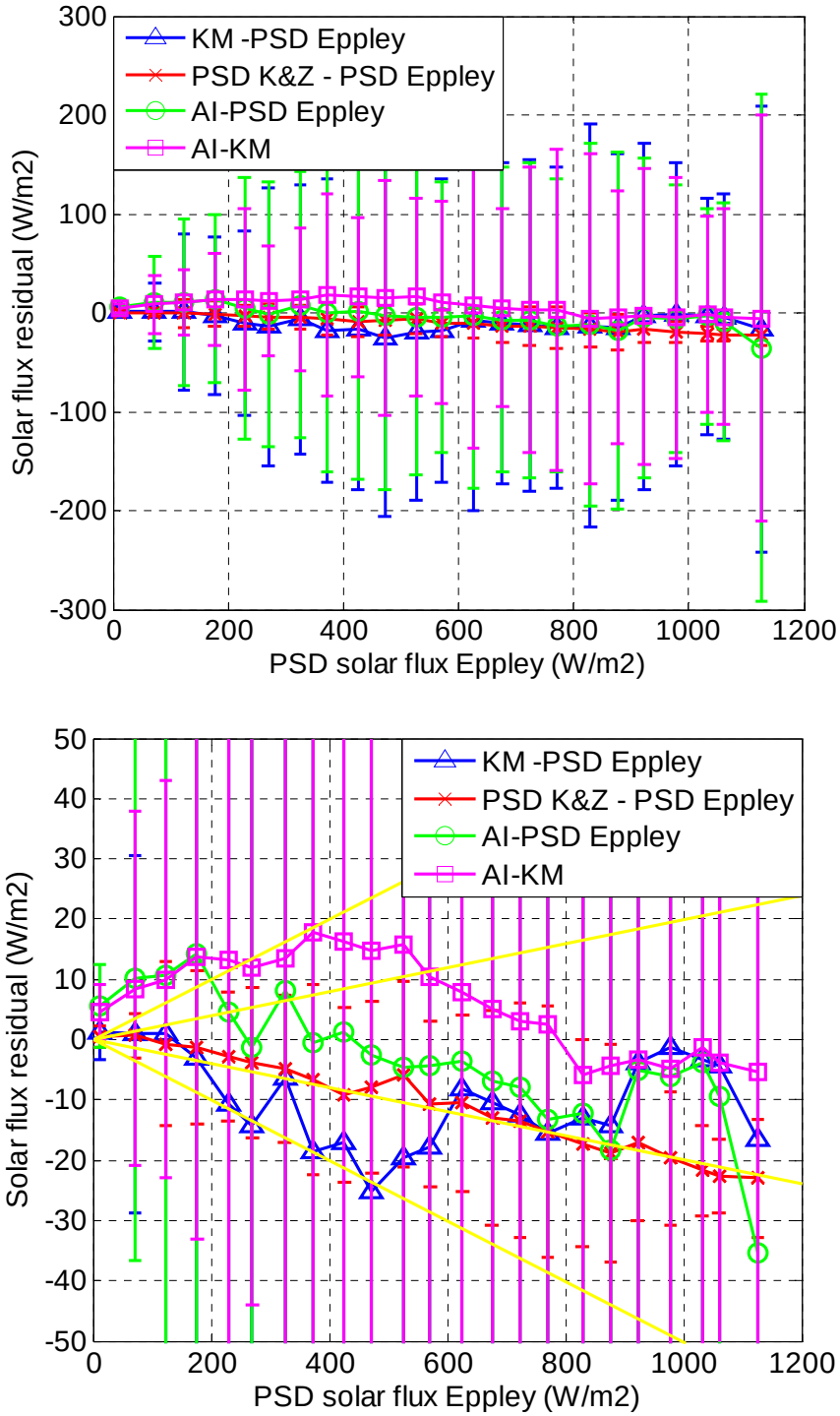

Figure 17. Dependence of shortwave residuals (instrument to compare minus PSD Eppley) on solar radiation for the ship (blue), the AutoIMET (green and magenta), and PSD (red). The lower panel is an expanded view of the top panel with the yellow lines indicating slope of ±2% and ±5%

e) Wind speed and direction

Wind speed residuals (instrument to compare minus PSD bow sonic) are represented as a function of relative wind direction on Figure 18. Data were averaged into one degree direction bins. The two ship propeller anemometers compare relatively well with the PSD sonic located at the bow tower. In the (-30°, 30°) range, the KM starboard unit and the PSD bridge sonic are within 0.2 $m.s^{-1}$ from the sonic unit, while the KM portside unit is higher at $0.4m.s^{-1}$. Due to its location, the AI sensor reads about -0.5 m.s-1 lower in the same range. Except for the AI and KM portside anemometers, the flow difference between the bridge and bow tower measurements is relatively the same in the (-30°, 30°) range, while it is accelerated from the portside (-60°, -30°) and slightly decelerated from the starboard side (30°, 60°). The AI unit has a similar pattern, but with more deceleration in the (-30°, 30°) range due to the ship structure.

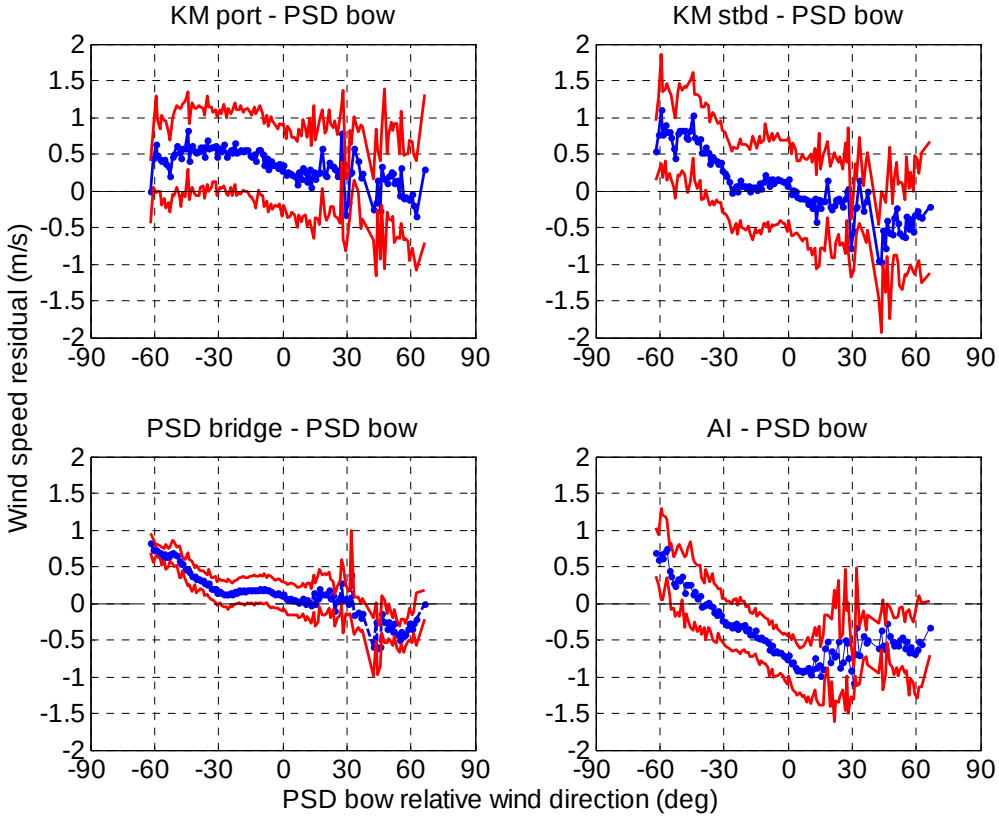

Figure 18. Wind speed residuals (instrument to compare minus PSD bow) as a function of ship relative wind direction. The four panels show the median (blue) and standard deviation (red). KM port and KM stbd refer to the ship anemometers (see Figure A1). AI refers to the IMET propeller (see Figure 5). PSD bow refers to the sonic located at the bow tower, and PSD bridge to the sonic located on the bridge.

Figure 19 is the same as Figure 18 but for wind direction residuals (defined as instrument to compare minus PSD bow). All three anemometers on the bridge agree well when the incident wind direction is directly over the bow of the ship, but the AI anemometer is about 10° off. Otherwise the wind difference between bridge and bow tower deviates up to +10° when the wind is from 30° portside and up to -10° when the wind is from 40° starboard side. Again the AI unit sees more dramatic direction deviations due to its deployment above the bridge roof. Additional results on flow distortion are presented in section 4.

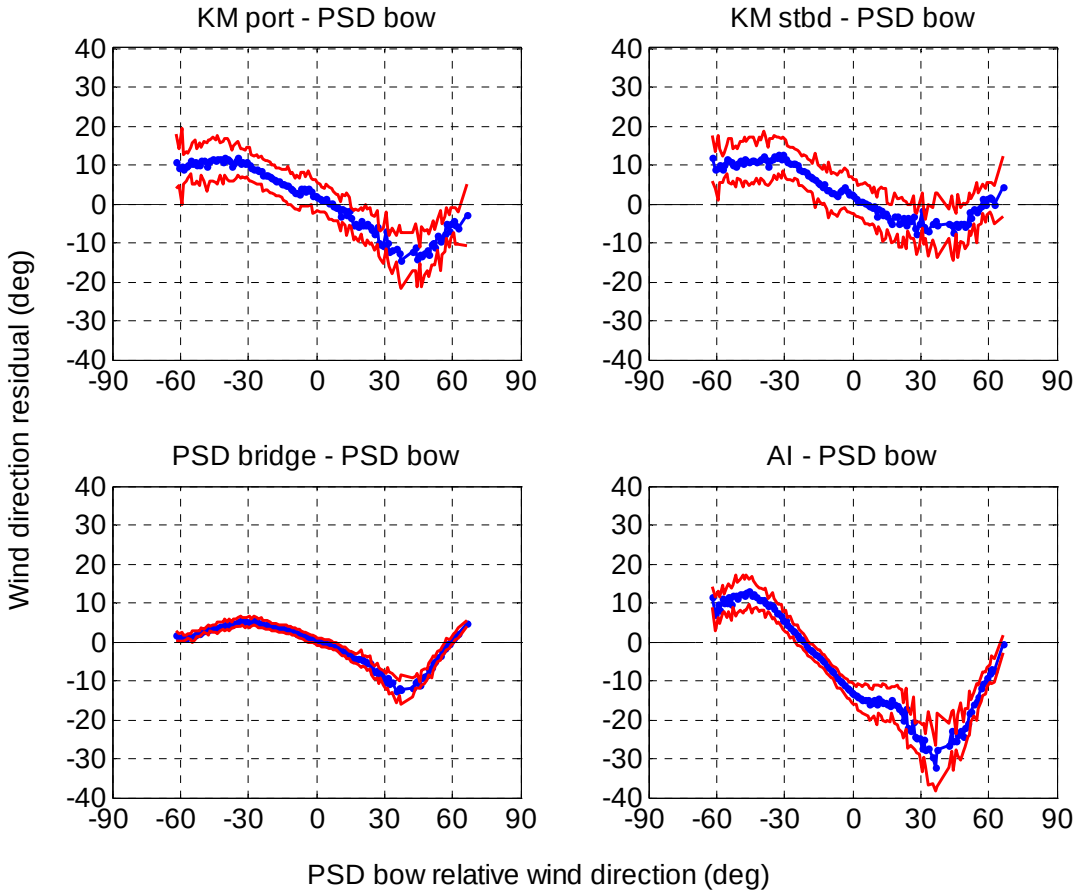

Figure 19. Wind direction residuals (instrument to compare minus PSD bow) as a function of ship relative wind direction. The four panels show the median (blue) and standard deviation (red).

5) WHOTS-5 buoy intercomparison

In this section, we compare the various instruments installed on the *Kilo Moana* with the WHOTS-5 buoy used as reference. The goal is to validate the previous comparisons, but also to assess the edited buoy data. Air temperature, relative humidity and wind speed variables were all adjusted to the reference height of the buoy sensors.

a) Air temperature

The residual (instrument to compare minus W5) values shown on Figure 20 are as follow: AI-W5 = - 0.08°C, PSD-W5 = -0.27°C, KMrot-W5= -1.32°C, KMrtd-W5= -0.74°C. The AI and PSD values agree well at night, but reach respectively about 0.08°C and 0.28°C higher during the day. This shows good agreement between AI and the buoy, and this especially after a year of unattended operation. The PSD unit seems to be ~0.2°C lower when compared to the buoy and AI units and this is probably due to the different enclosures used (aspirated shield versus naturally ventilated shield). This graph confirms also that the two ship units are reading too low.

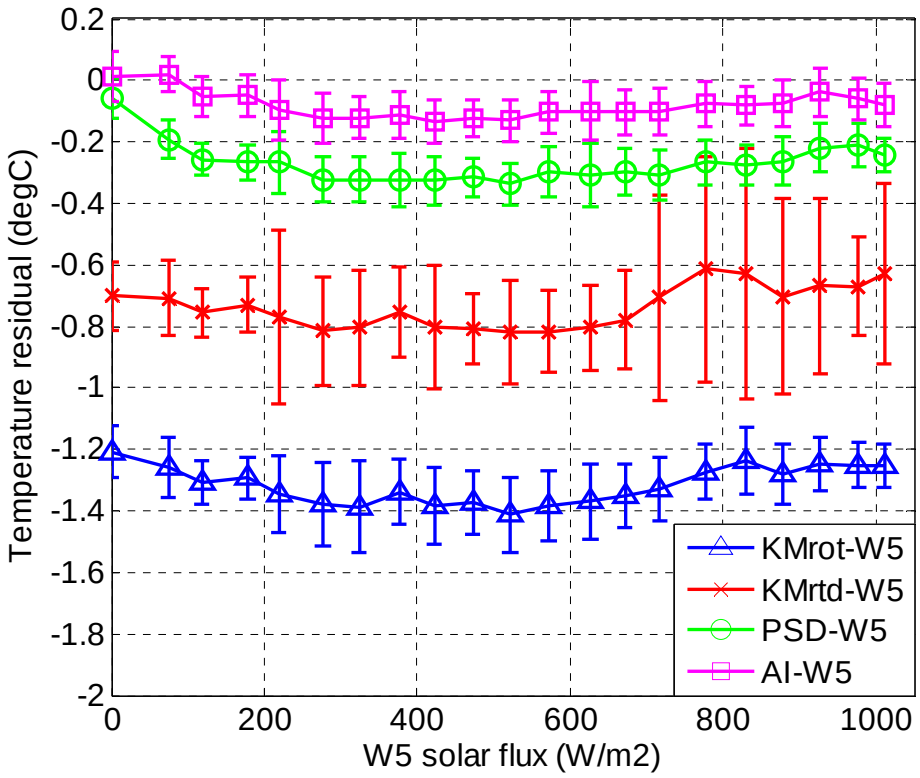

Figure 20. Dependence of air temperature residuals on solar radiation for the two ship sensors (blue and red), the AutoIMET (magenta) and PSD (green).

b) Relative humidity

The residual values shown on Figure 21 are as follow: KMrot-W5= 0.99%, AI-W5 = 2.84%, PSD-W5 = 1.96%. In this comparison, it appears that the rotronics air humidity unit of the KM is closer to the buoy value compare to PSD or AI units. Nonetheless, all instruments follow one another closely within an envelope about 2% wide.

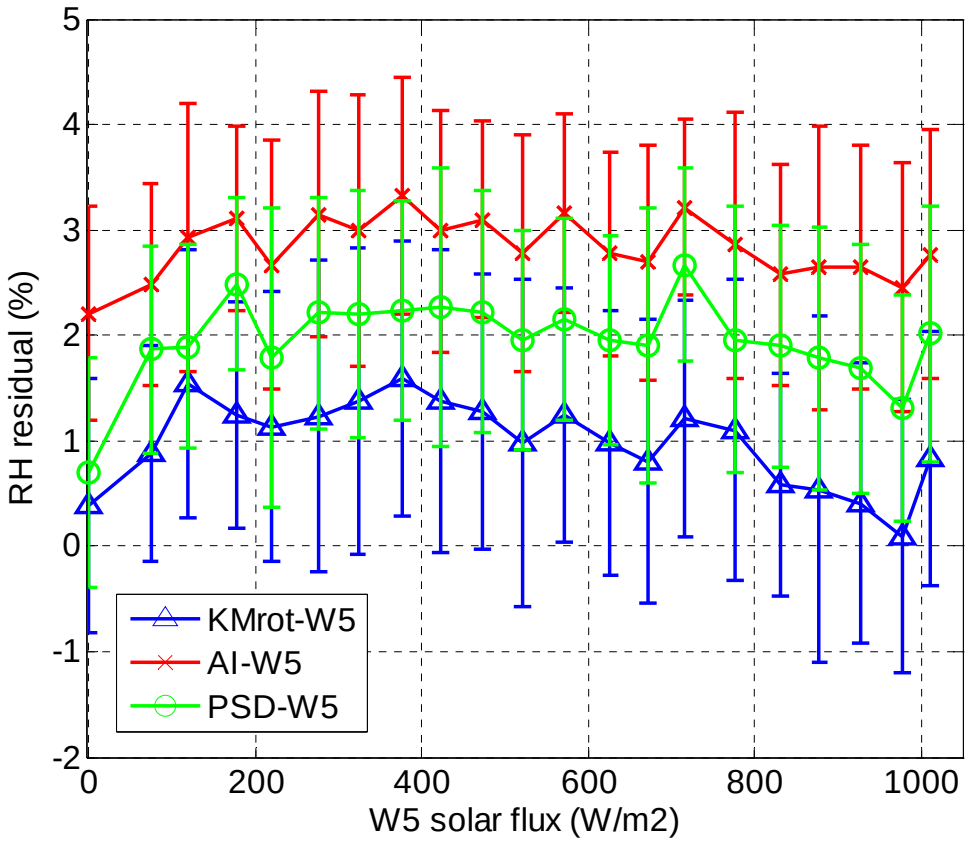

Figure 21. Relative humidity residuals as a function of solar radiation for the ship sensor (blue), the AutoIMET (red) and PSD (green).

c) Sea temperature

Figure 22 shows that the ship's thermosalinograph and the buoy sensor are in very good agreement. Due to its depth, the PSD seasnake captures the daytime surface warming and reads about 0.1°C at the solar peak. During the night, the KM and PSD sensors agree well and read about a tenth of a degree higher than the buoy.

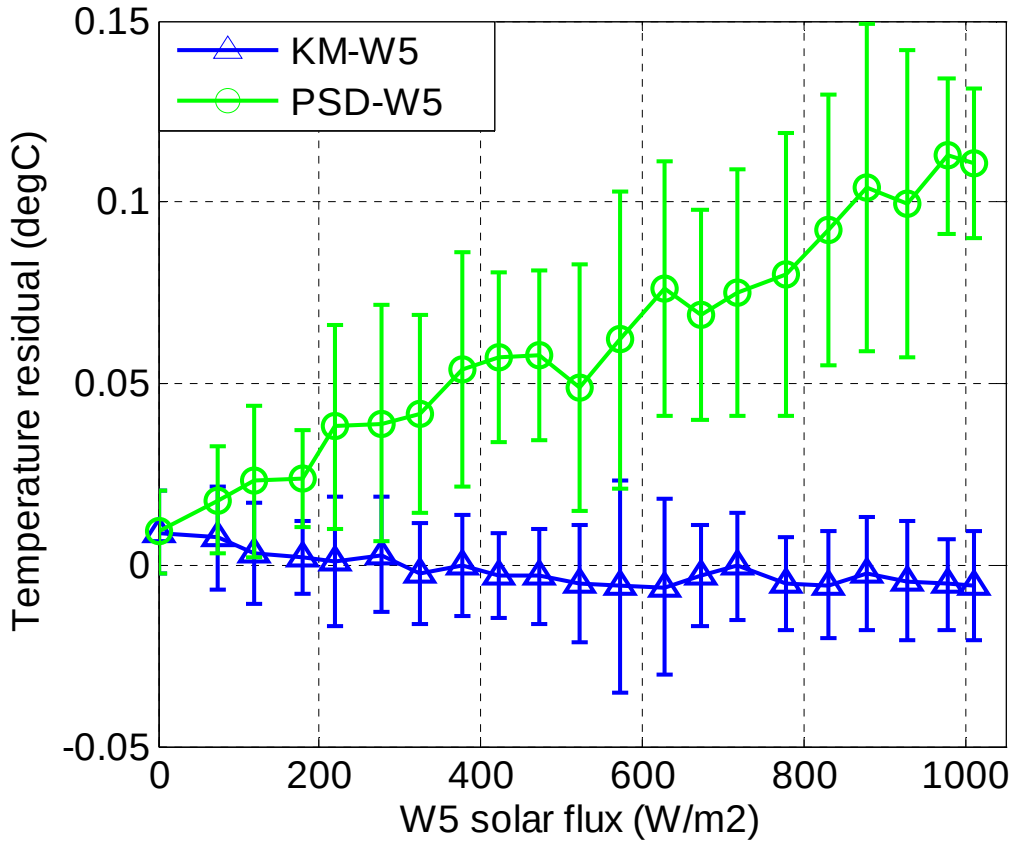

Figure 22. Dependence of sea surface temperature residual as a function of solar radiation for the ship sensor (blue) and PSD (green).

d) Longwave and shortwave radiation

Comparisons of the pyrgeometers on the ship with the units on the buoy reveal that the PSD Eppley is in close agreement with the buoy in the low range while the other units all read higher (Figure 23). By looking at the longwave radiation residual (instrument – W5) as a function of solar radiation (Figure 24), we can see that the differences with the buoy are diverse for each instrument. The PSD reads about 5 $W.m^{-2}$ lower than the buoy at the solar peak while the KM is about 3 $W.m^{-2}$ lower. The PSD Kipp&Zonen and AI pyrgeometers are relatively constant in the 200-800 $W.m^{-2}$ range at about 4 $W.m^{-2}$ and 5$W.m^{-2}$ above the buoy respectively. This graph reinforces that the KM unit is constantly about 2 $W.m^{-2}$ higher than the PSD Eppley, while the PSD Kipp&Zonen and AI pyrgeometers suffer from problems of shortwave contaminations (+6 $W.m^{-2}$ and +10 $W.m^{-2}$ higher than PSD during the day as mentioned previously).

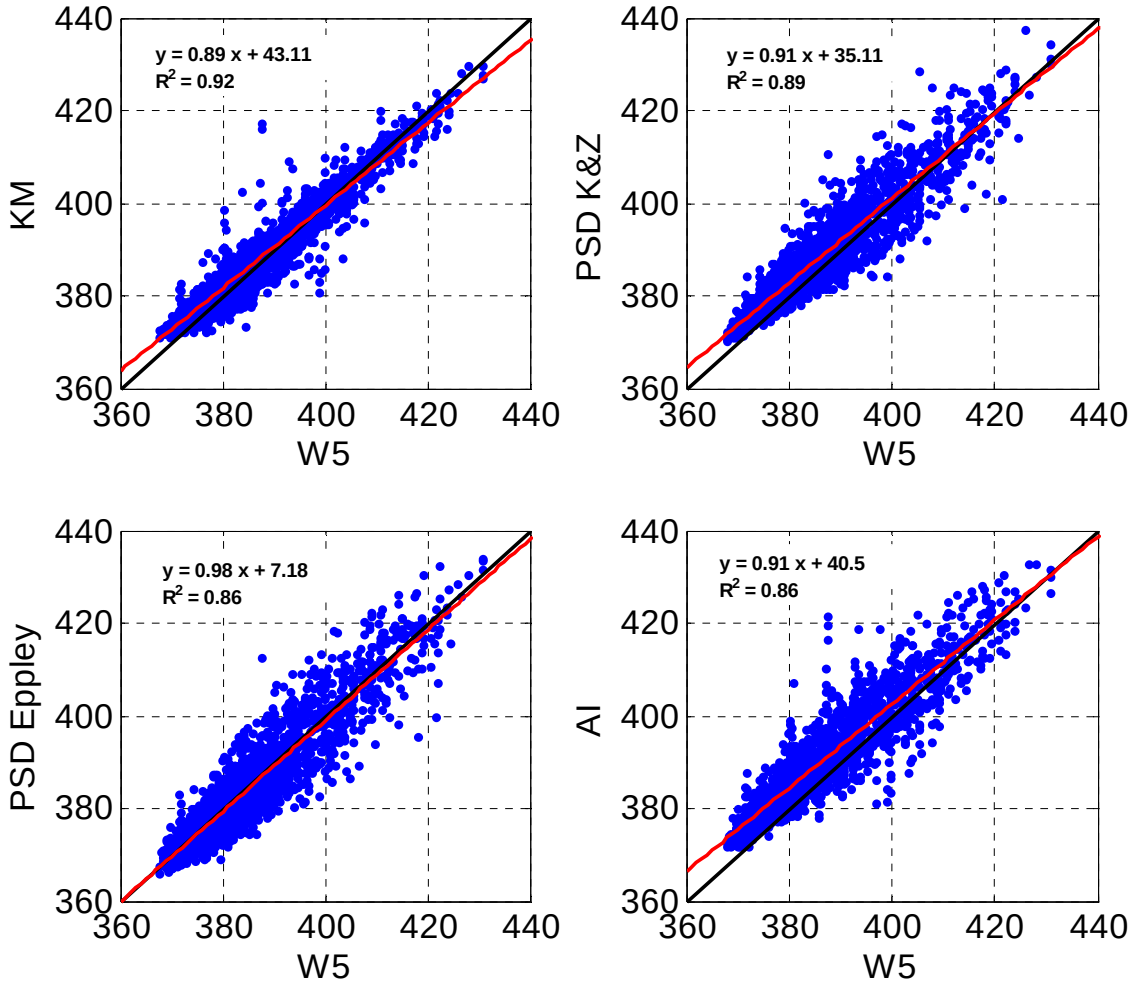

Figure 23. Comparison plots of longwave radiation for the ship, AutoIMET, PSD and the buoy W5. The equations and squared correlation coefficients are indicated for each linear regression (red), and the black line indicates a 1:1 ratio.

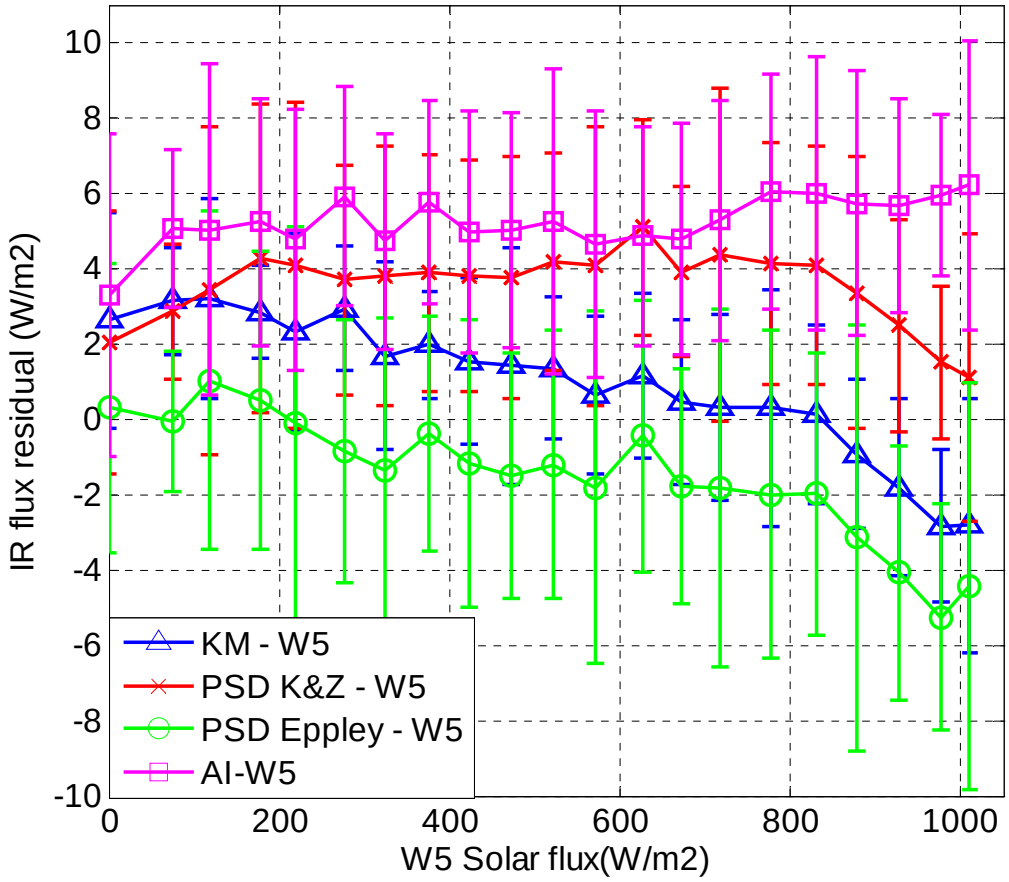

Figure 24. Dependence of longwave residuals on solar radiation for the ship (blue), PSD (red and green), and the AutoIMET (magenta).

A look at the shortwave measurements from the ship on figures 25 and 26 show that they all differ from the buoy measurement by about 5% at the diurnal solar peak. Several factors might contribute to these differences. The dome of the buoy pyranometers became probably contaminated with salt after a year of unattended operation at sea, and the measurements onboard the ship might be affected by various ship interferences. The different cloud conditions also cause these comparisons to be more difficult to understand. Differences can also be observed between the various instruments on the ship, but this does not reproduce exactly all differences from the previous comparison (Figure 17).

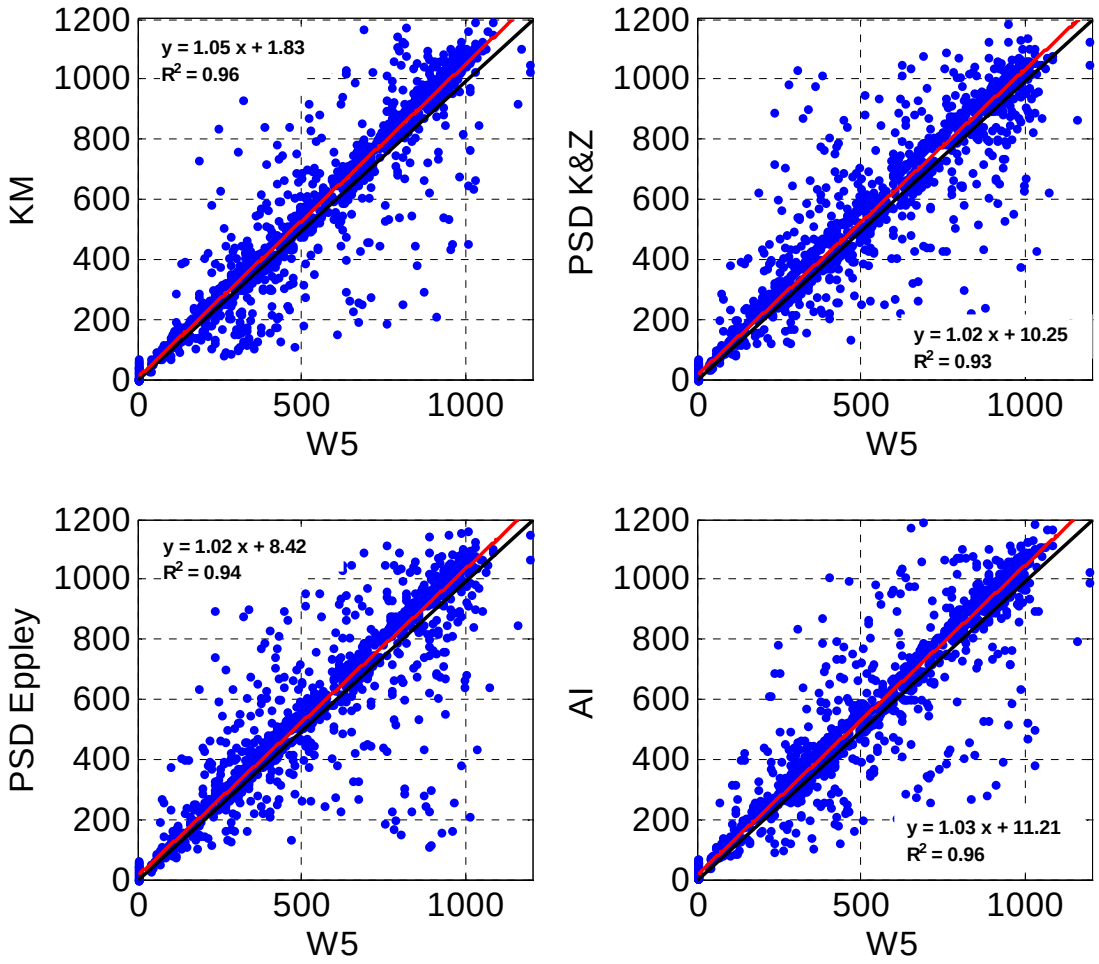

Figure 25. Comparison plots of shortwave radiation between the ship, AutoIMET, PSD and the WHOTS-5 buoy. The equations and squared correlation coefficients are indicated for each linear regression (red), and the black line indicates a 1:1 ratio.

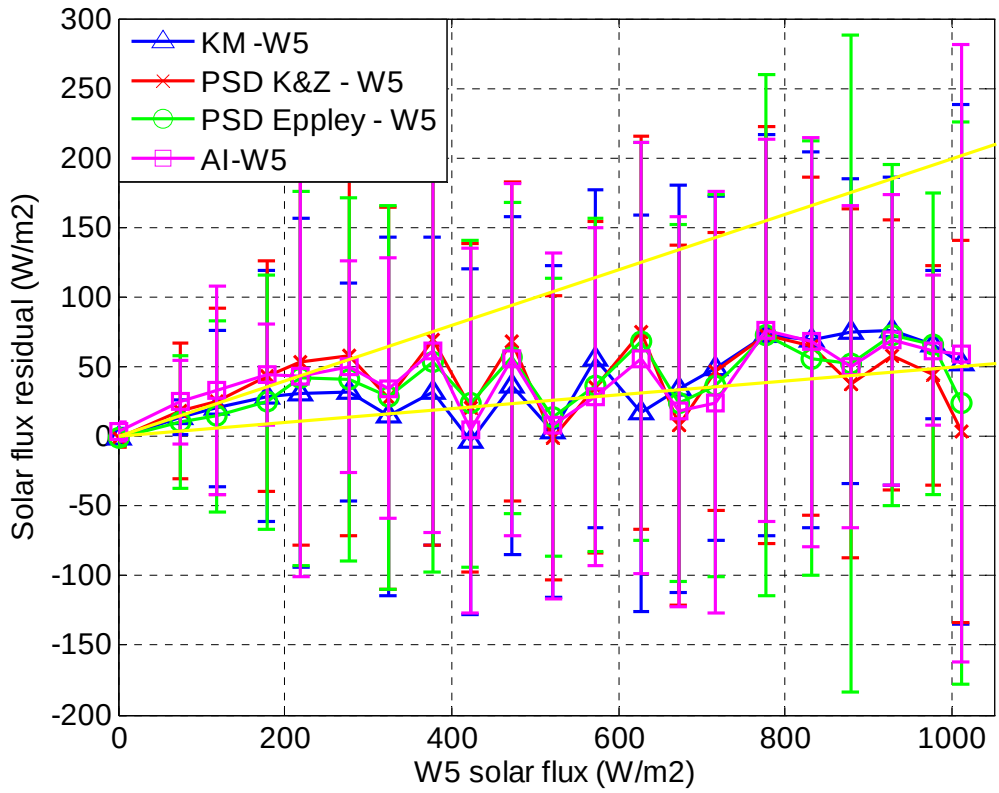

Figure 26. Dependence of shortwave residuals on solar radiation for the ship (blue), PSD (red and green), and the AutoIMET (magenta). The yellow lines indicating slope of +5% and +20%

e) Wind speed and direction

A quick look at wind speed residuals (instrument to compare minus W5) on Figure 27 confirms some results mentioned with Figure 18. Both PSD sonics and the KM starboard anemometer are in close agreement, but read about 0.3 $m.s^{-1}$ lower. The ship was heading about ~ 90° in that inter-comparison period so this corresponds to (-30°, 5°) range in relative wind direction. The KM portside anemometer reads about 0.3 $m.s^{-1}$ higher in this range, making it match perfectly with the buoy measurement while the AI unit measures a slower wind at its location. As shown on Figure 28, the wind direction from WHOTS-5 buoy appears to present some issues. The WHOTS-5 anemometer had failed by the time of the recovery cruise and the other unit had direction biases due to bird wires being too close, so wind direction between ship measurements and buoy will be evaluated with WHOTS-6 buoy.

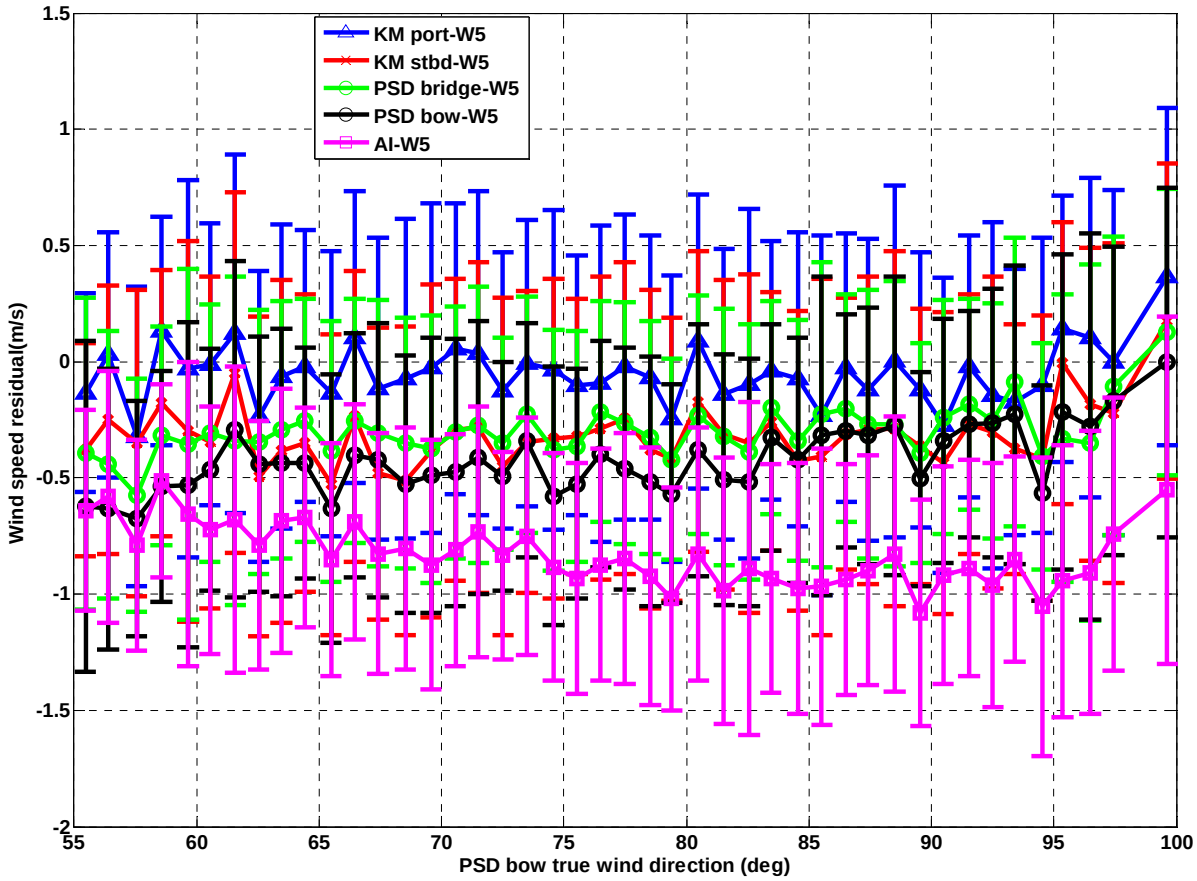

Figure 27. True wind speed residuals (instrument – W5) as a function of the PSD bow true wind direction. Data were averaged into one degree direction bins, and a minimum of 10 points in the average were required.

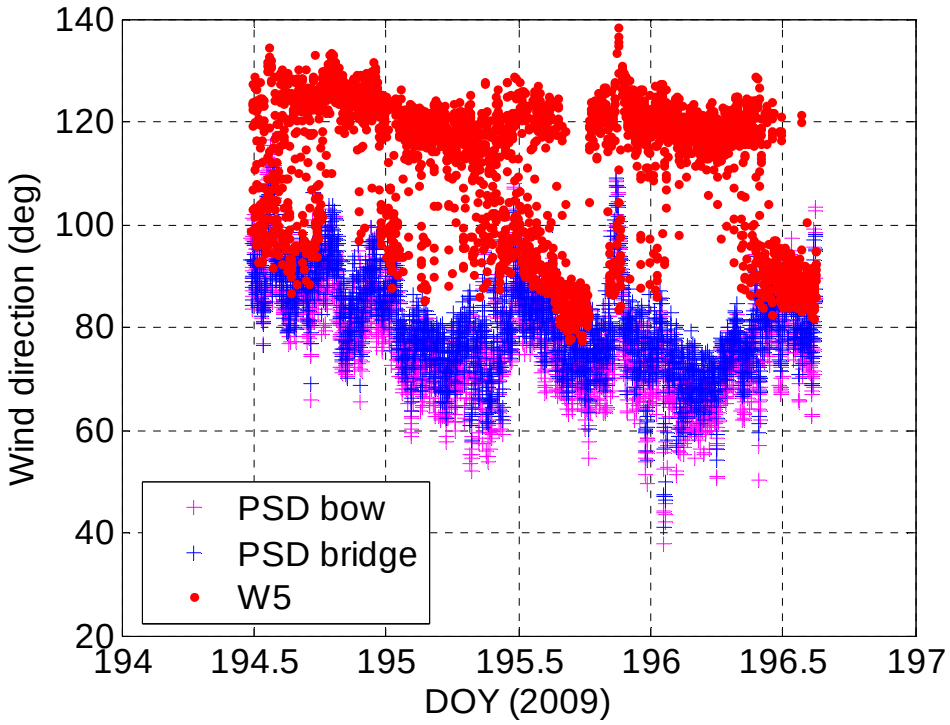

Figure 28. Time series of true wind direction at 3.255m between the two PSD sonic and the buoy edited data.

6) WHOTS-6 buoy intercomparison

In this section, we compare the various instruments installed on the *Kilo Moana* with the WHOTS-6 buoy used as reference (W6_7 logger). Here we expect the comparison results to be more accurate, as the WHOTS-6 buoy was freshly deployed. Air temperature, relative humidity and wind speed variables were all adjusted to the reference height of the buoy sensors.

a) Air temperature

The residual values (instrument to compare minus W6_7) shown on Figure 29 are as follow: KMrot-W6_7= -1.99°C, KMrtd- W6_7= -1.43°C, PSD- W6_7 = -0.93°C, AI- W6_7 = -0.74°C and W6_19- W6_7 = - 0.52°C. This confirms the previous differences revealed before with the exception that one of WHOTS-6 sensor (W6_7) is reading ~0.5°C higher than the other (W6_19), but no explanation could be found to that problem when noticed during deployment.

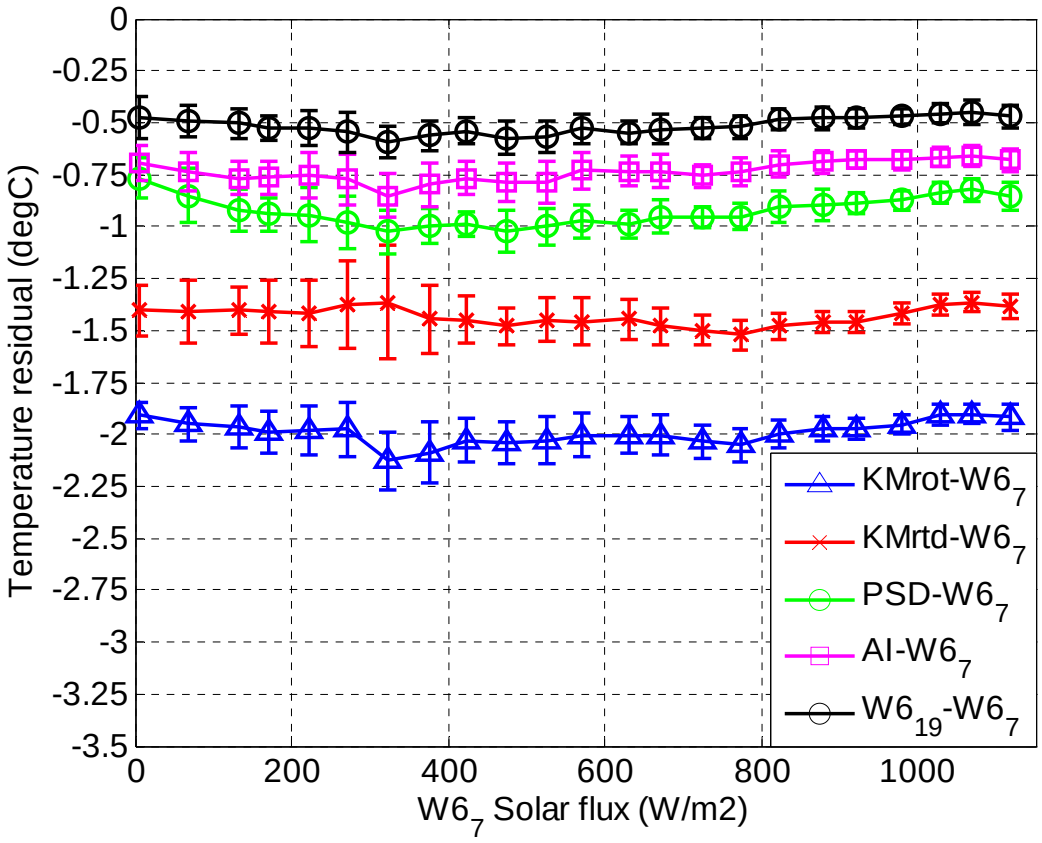

Figure 29. Dependence of air temperature residuals (instrument to compare minus W6_7) on solar radiation for the two ship sensors (blue and red), PSD (green), the AutoIMET (magenta) and WHOTS-6 buoy (black). W6_7 and W6_19 refer to the loggers 7 and 19 on WHOTS-6 buoy.

b) Relative humidity

The residual values shown on Figure 30 are as follow: KMrot-W6_7= -0.79%, AI- W6_7 = 0.87%, PSD- W6_7 = 0.07%, W6_19 - W6_7 = 0.64%. This comparison confirms that all instruments follow one another closely within a 2% envelope. Note also that this comparison reveals that the humidity sensor of WHOTS-5 buoy was reading about 2% lower after a year of unattended operations since in that plot the envelope is centered on 0%, while it was around 2% in the WHOTS-5 buoy comparison.

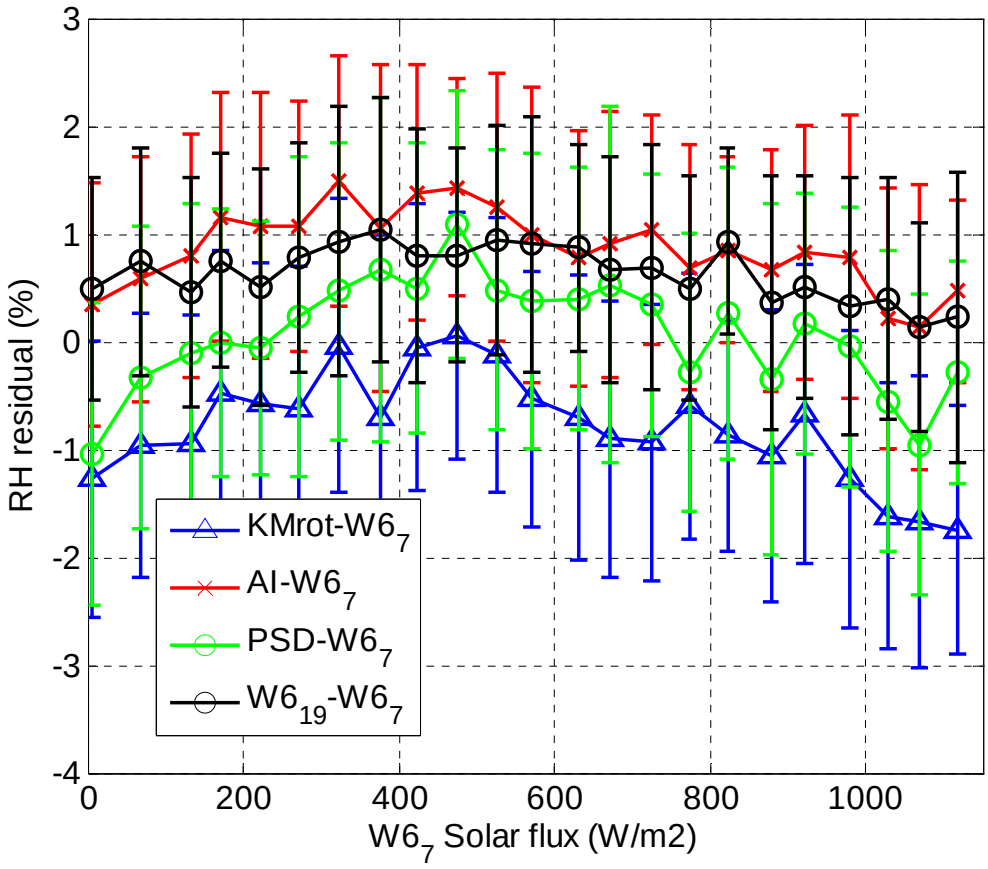

Figure 30. Relative humidity residuals (instrument to compare minus W6_7) as a function of W6_7 solar radiation for KM (blue), the AutoIMET (red), PSD (green) and WHOTS-6 buoy (black).

c) Sea temperature

Both buoy's sea temperature sensors are in excellent agreement. As found previously, the ship's thermosalinograph follows closely the buoy measurements, while the PSD seasnake shows evidence of diurnal warming.

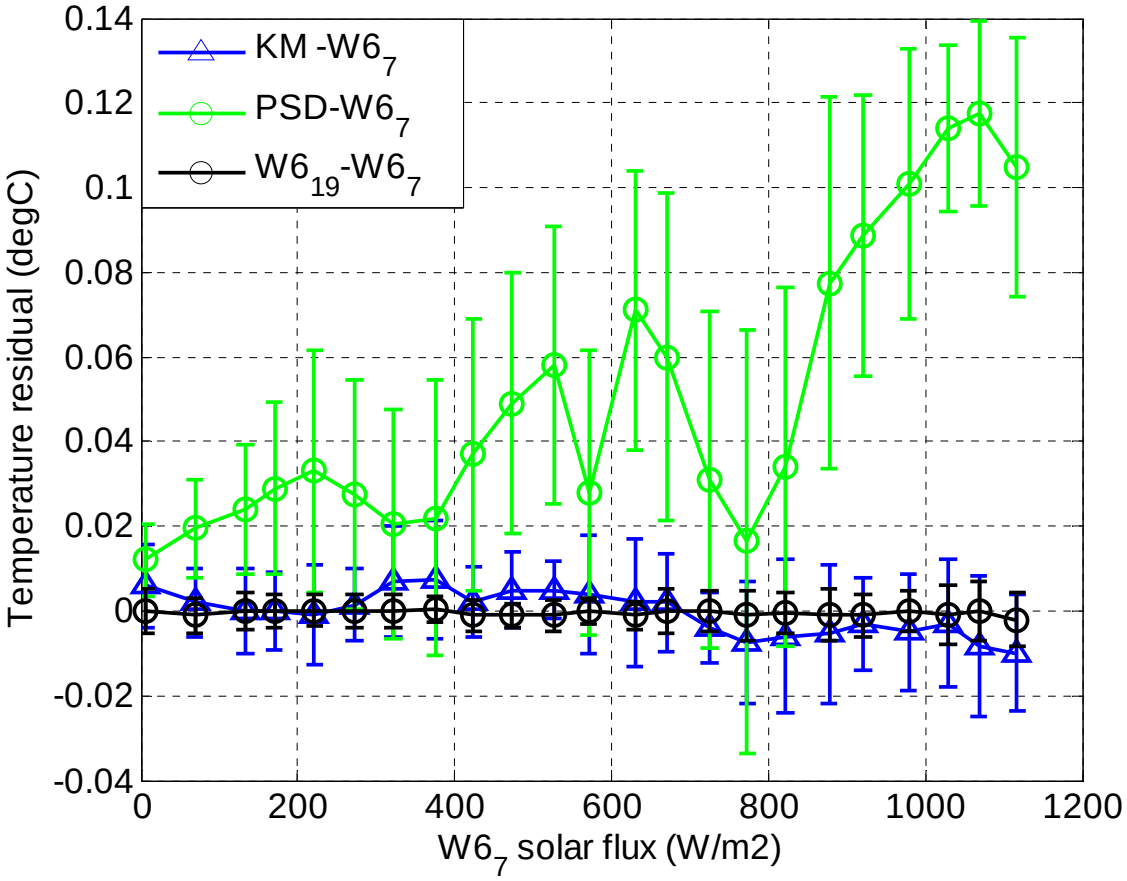

Figure 31. Dependence of sea surface temperature residual as a function of solar radiation for the ship sensor (blue), PSD (green) and WHOTS-6 buoy (black).

d) Longwave and shortwave radiation

Comparisons of the pyrgeometers on the ship with the WHOTS-6 units confirm again that the PSD Eppley is in close agreement with the buoy (Figure 32). The two buoy units track also each other very well and present a strong correlation. The longwave radiation residual (instrument – W6_7) shown on Figure 33 are as follow: KM - W6_7= 0.72 W.m^{-2}, PSD_K&Z= 1.21 W.m^{-2}, PSD Eppley - W6_7 = 0.06W.m^{-2}, AI- W6_7 = 2.83 W.m^{-2}, W6_19 - W6_7 = 1.40 W.m^{-2}. The PSD Eppley unit is in close agreement, while the others show slightly higher measurement at low IR values indicating some possible shortwave contaminations.

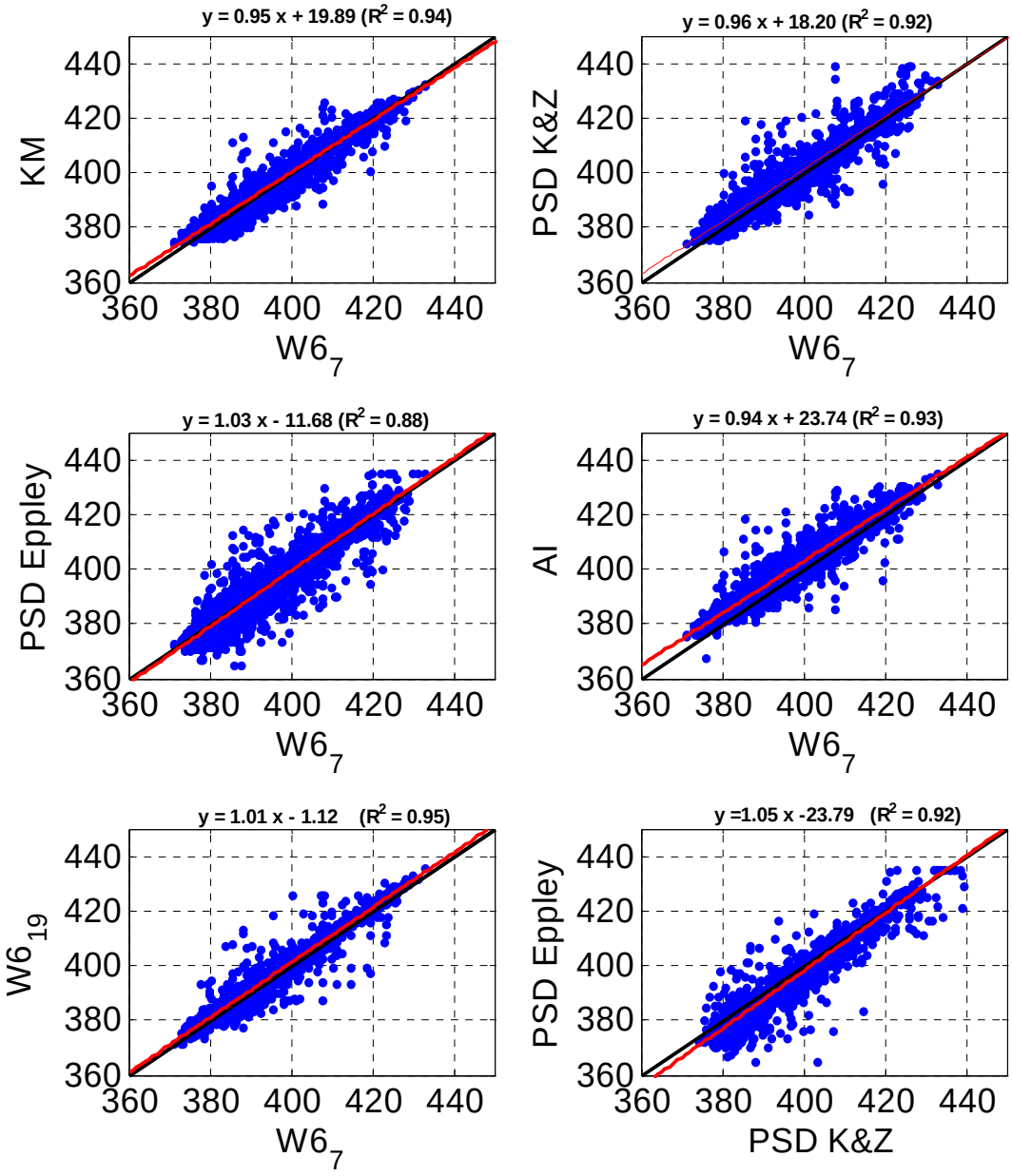

Figure 32. Comparison plots of longwave radiation for the ship, AutoIMET, PSD and the buoy W6. The equations and squared correlation coefficients are indicated for each linear regression (red), and the black line indicates a 1:1 ratio.

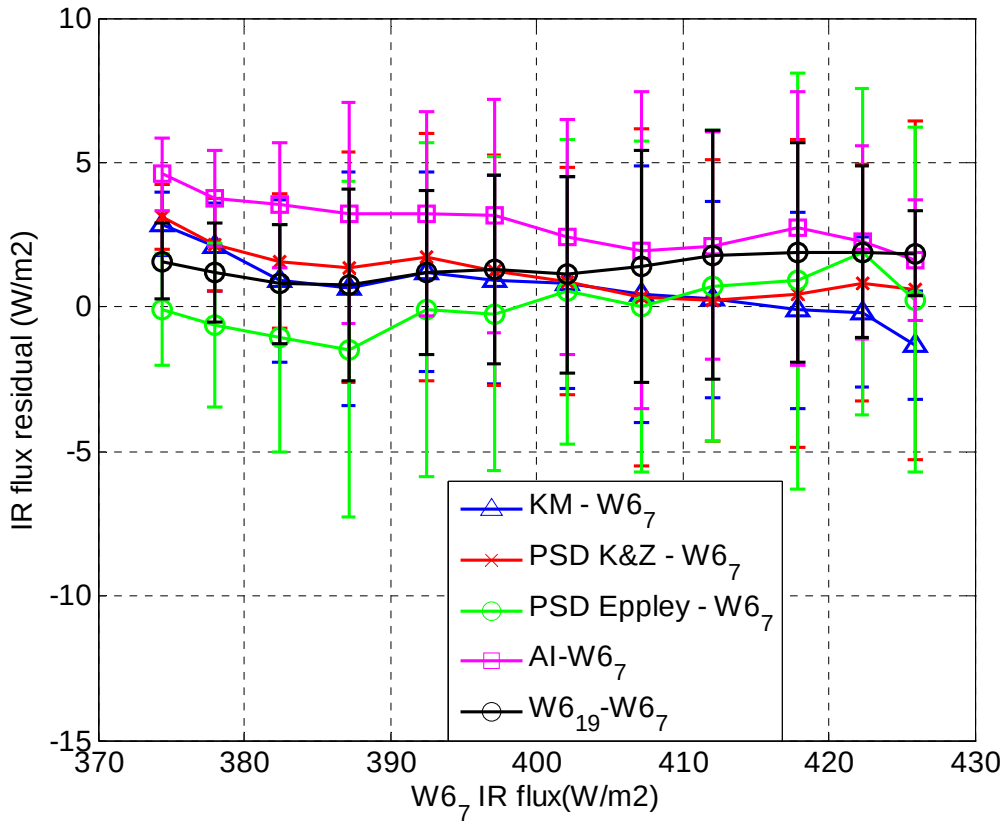

Figure 33. Dependence of longwave residuals on solar radiation for the ship (blue), PSD (red and green), and the AutoIMET (magenta).

Similarly for the shortwave measurements from the ship, Figures 34 show reasonable agreements between various units. Looking at the shortwave radiation residuals (instrument – W6_7) on Figure 35 indicates however similar features noticed on Figure 17. The averaged residuals are as follow: KM-W6_7= -10.79 W.m^{-2}, PSD_K&Z= -7.97 W.m^{-2}, PSD Eppley - W6_7 = 2.64 W.m^{-2}, AI- W6_7 = -1.55 W.m^{-2}, W6_19 - W6_7 = -14.34W.m^{-2}. The PSD Eppley and AI units are in good agreement with the W6_7 sensor, while the PSD K&Z reads higher at solar peak. The KM and W6_19 units are reading lower in the 200-800 W.m^{-2} range. All units, except AI, are measuring the same at night.

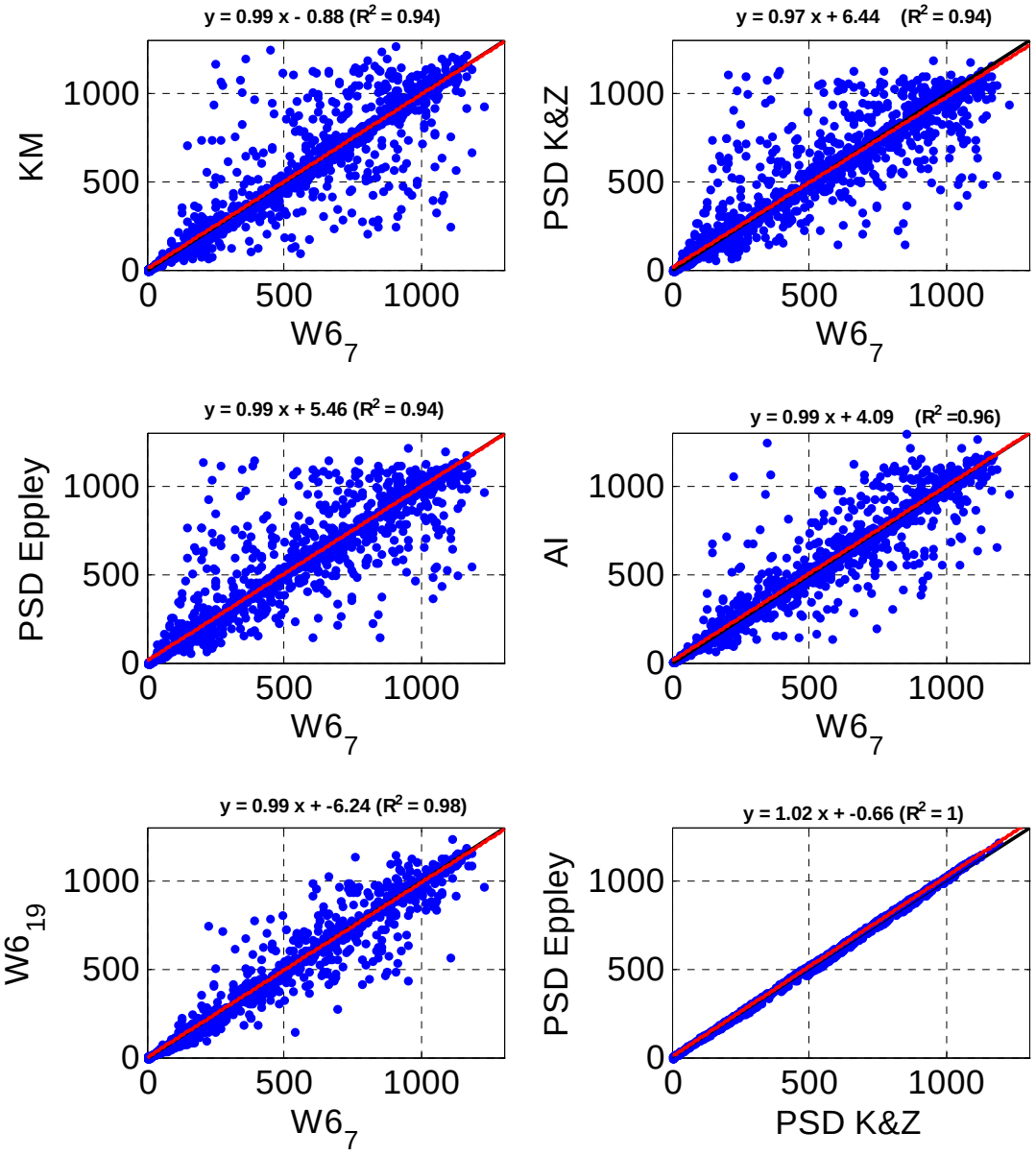

Figure 34. Comparison plots of shortwave radiation between the ship, AutoIMET, PSD and the WHOTS-6 buoy. The equations and squared correlation coefficients are indicated for each linear regression (red), and the black line indicates a 1:1 ratio.

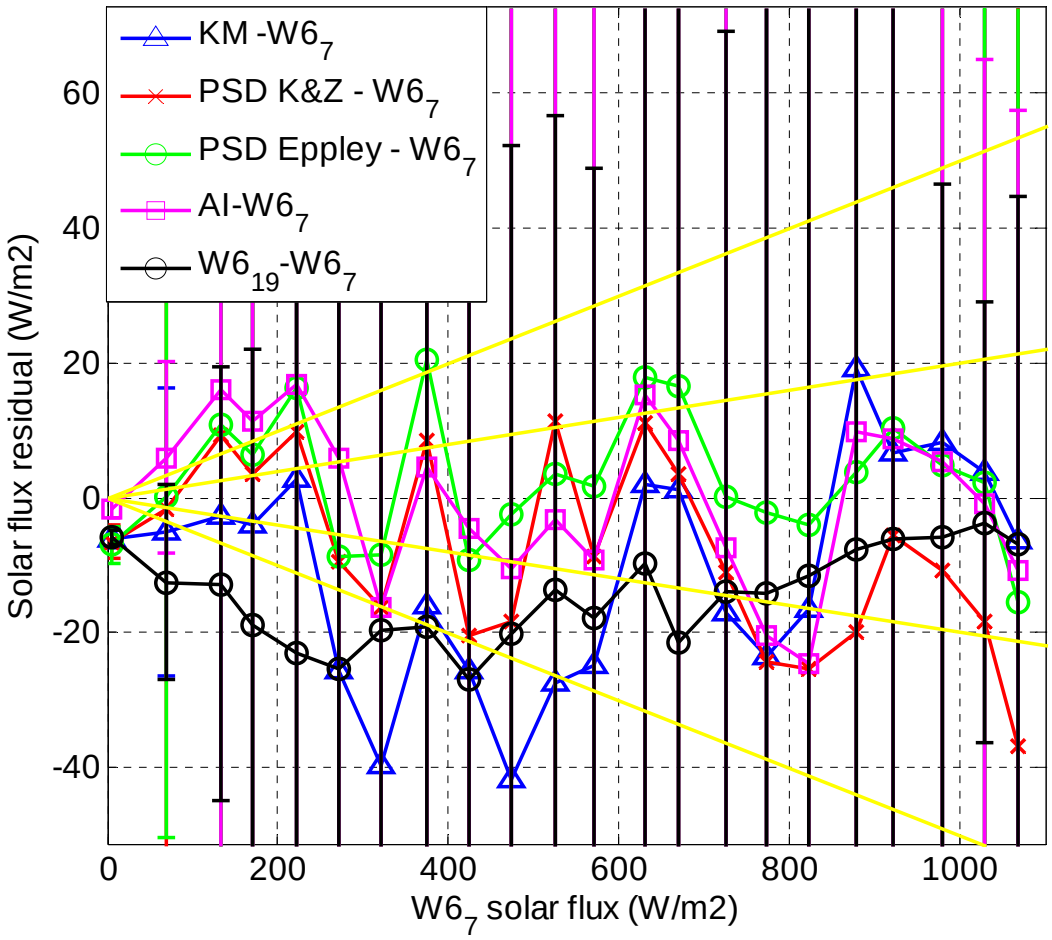

Figure 35. Dependence of shortwave residuals as a function of W6_7 solar radiation for the ship (blue), PSD (red and green), the AutoIMET (magenta), and the buoy (black). This graph is a an expanded view with the yellow lines indicating slope of ±2% and ±5%

e) Wind speed and direction

Figure 36 shows the wind speed residuals (instrument – W6_7) as a function of true wind direction from W6_7. Data were averaged into one degree direction bins. The averaged wind speed residuals presented on are as follow: KMport-W6_7= 0 $m.s^{-1}$, KM stbd – W6_7 = -0.32 $m.s^{-1}$, PSD bridge – W6_7 = -0.21 $m.s^{-1}$, PSD bow – W6_7 = -0.38 $m.s^{-1}$, AI- W6_7 = -0.83 $m.s^{-1}$, W6_19 - W6_7 = -0.04 $m.s^{-1}$. Similar to the comparison with WHOTS-5 buoy, we can see that both PSD sonics and the KM starboard anemometer are in close agreement, but read about 0.3 $m.s^{-1}$ lower compare to W6_7. The AI unit measures about 0.4 $m.s^{-1}$ lower winds. The two buoy anemometers agree well, but seem to diverge slightly at 100° direction. The

KM portside anemometer reads about 0.3 $m.s^{-1}$ higher than the KM starboard unit, resulting in perfect agreement with the buoy measurements.

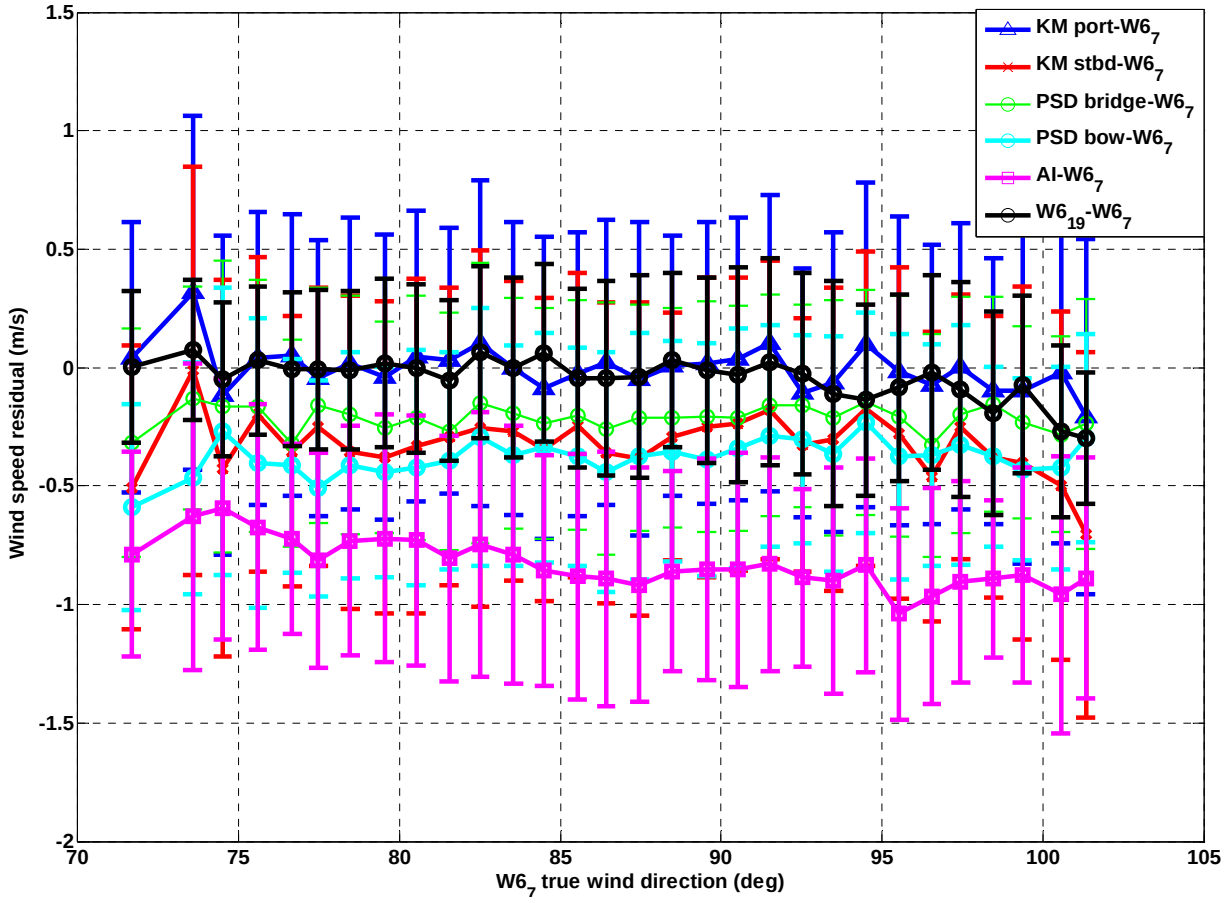

Figure 36. True wind speed residuals (instrument – W6_7) as a function of true wind direction. Data were averaged into one degree direction bins, and a minimum of 10 points in the average were required.

Figure 37 shows the wind direction residuals (instrument – W6_7) as a function of true wind direction from W6_7. Clearly the effect of flow distortion can be seen on this graph. While the PSD bow sonic is in very good agreement with W6_7 anemometer, the other units diverge. During that comparison period the ship heading was about ~ 100°, and we can see that when the wind blows directly over the bow, both PSD sonics and KM units follow closely while the AI deviates up to -10°. At about 70° (equivalent to 30° in relative wind direction), the three bridge anemometers as well as the AI units are showing a deviated

direction from 5° up to 10° which confirms the results presented in section 4. Interestingly the W6_19 direction also seems to deviate slightly by ~5° when the wind is from 100°.

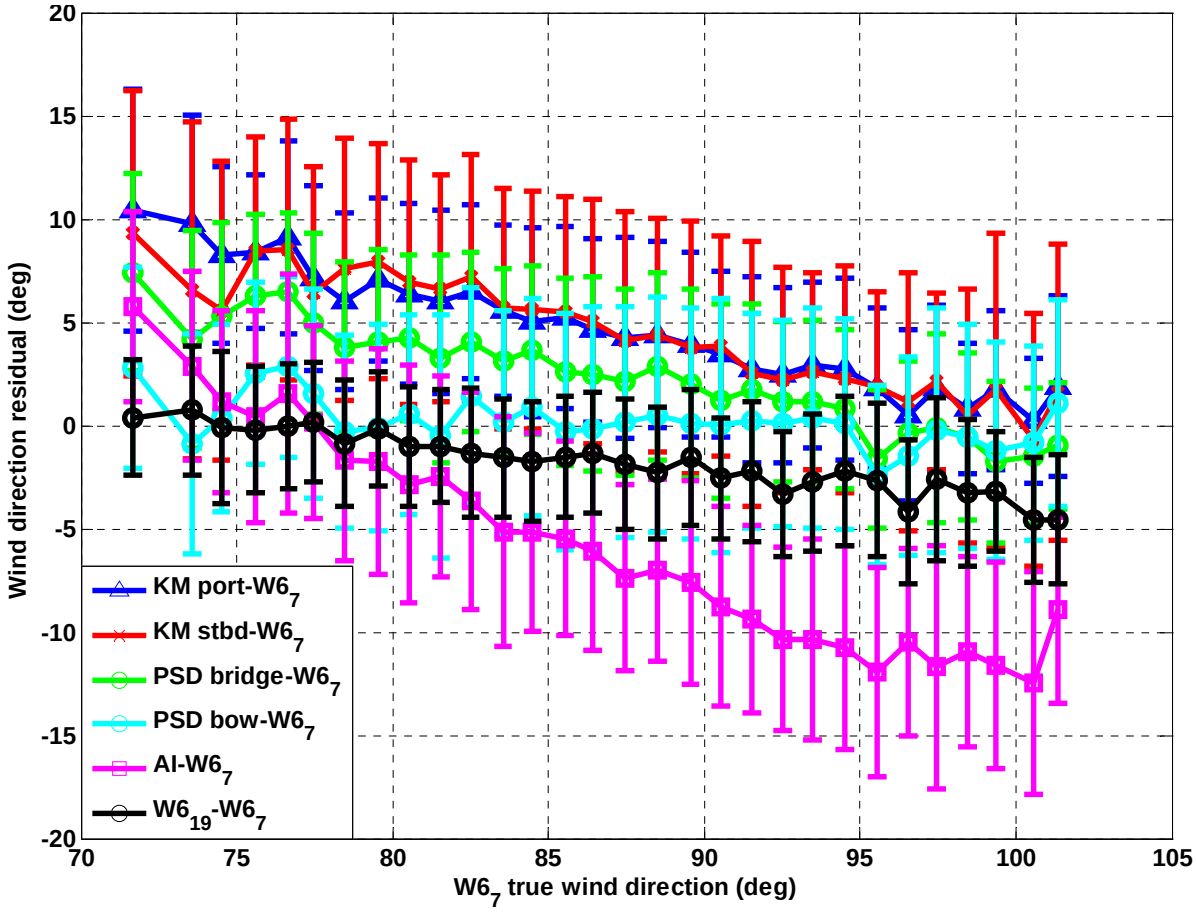

Figure 37. True wind direction residuals (instrument – W6_7) as a function of true wind direction. Data were averaged into one degree direction bins, and a minimum of 10 points in the average were required.

7) Wind flow distortion

The previous comparisons of the wind measurements from the ship with those made from the buoys revealed already some flow distortion effects of the *Kilo Moana*. From Figures 36 and 37, one can say that those effects are not that different between wind speed measurements from the bow tower and bridge locations. Discrepancies in the wind direction can however be observed when the wind is from the port side, while they agree relatively well for incident

wind directions over the bow of the ship. However another difficulty arises on the *Kilo Moana* structure, and it concerns the upward deflection of the upwind flow. As an illustration, Figure 38 shows the tilt of the flow over the superstructure of the KM as a function of relative wind direction (0° meaning a flow coming directly over the bow). As expected, this graph reveals that the distortion is considerably more important at the ship bridge mast than at the bow tower. When the flow direction is directly over the bow of the KM, the wind is deflected upward by about 20° at the ship's mast and ~5° at the bow tower. Significant reduction in the distortion of the flow is apparent when winds are from either the port or starboard sides. These data seem to show some outlier regimes at ~15° for the ship's bridge and ~2-3° for the bow tower. No plausible explanation was yet found to explain this.

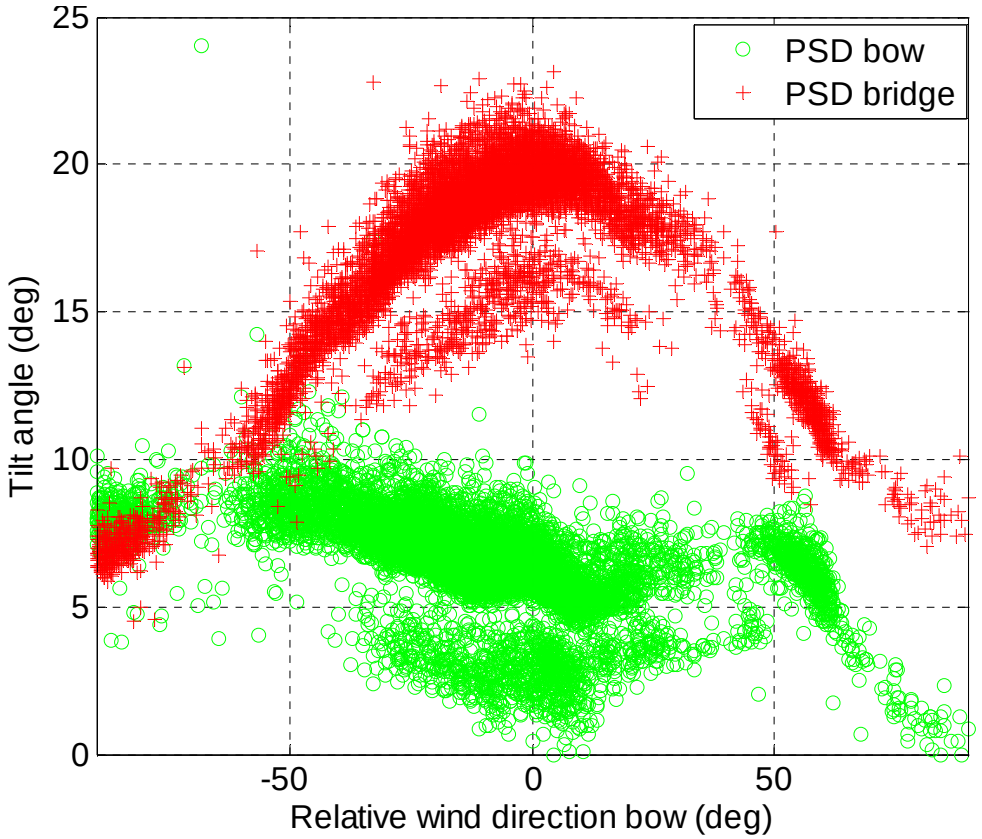

Figure 38. Tilt of streamwise wind over the ship for direction between -90° portside and +90° starboard. Red '+' are from the PSD sonic at the ship's bridge, where the green 'o' are from the PSD sonic at the bow tower. Data represented are from doy 191 to 198.

When computing the eddy covariance fluxes for this cruise, the wind coordinate system were rotated with the mean streamwise wind in order to correct for the wind flow effects. In addition, corrections to the sonic relative wind components have been applied in order to

reduce the flow distortion effects when the ship's course changes. The coefficients were found by comparison with the buoy measurements and using minimization methods to reduce the distortion effects as illustrated on Figure 39. The blue trace shows the true wind speed computed from the PSD bridge with a distortion correction applied to it, while the red trace represents the KM portside anemometer uncorrected. The ship's speed is represented in green and shows when the *Kilo Moana* moved from WHOTS-6 to WHOTS-5 mooring at 194.45. The flow distortion effect can be observed on the uncorrected anemometer.

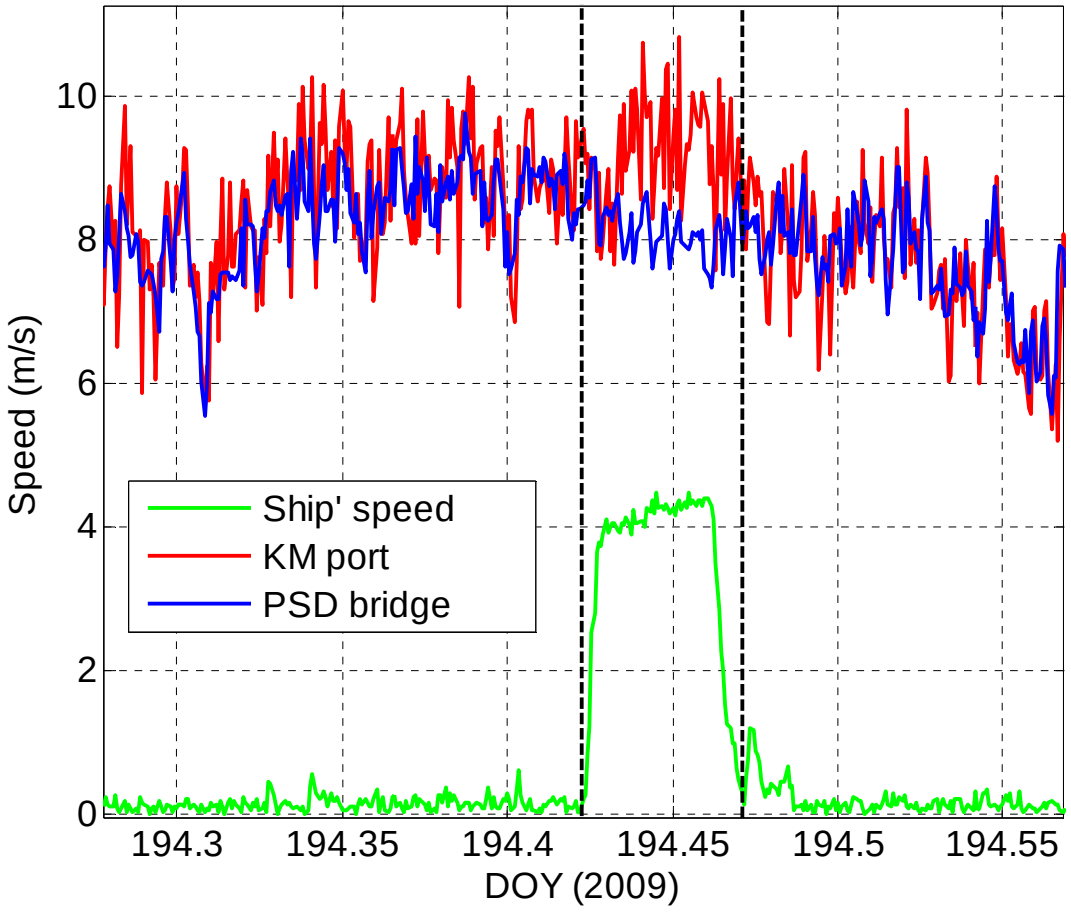

Figure 39. Illustration of flow distortion when the KM moved from WHOTS-6 to WHOTS-5 buoy at 194.45. The red trace is the uncorrected KM portside anemometer, while the blue line is the PSD bridge sonic corrected for flow distortion.

8) Summary

An evaluation of various meteorological sensors from both the *Kilo Moana* and buoys was performed for the 2009 WHOTS-6 Field Program.

Results show that the KM Rotronics temperature unit reads about 1.1 ºC too low and the KM RTD 0.5 ºC low when compared to the PSD instrument. The AI temperature unit was found to be in very good agreement with the WHOTS-5 buoy but reading about 0.2 ºC higher than PSD instrument. The difference is probably attributed to the type of enclosure used. One of the WHOTS-6 sensors was also found to read about 0.5 ºC too high.

The humidity sensors were found to be within an envelope about 2% wide when compared to the buoy measurements. However, the WHOTS-5 buoy unit was found to read about 2% lower after a year of unattended operations.

The KM corrected thermosalinograph agrees very closely with the sea temperature sensors on the buoys, while the PSD seasnake captures the daily sea surface warming.

The measurements between pyrgeometers deployed on the ship and the buoys are all within 5 $W.m^{-2}$ from each other. Solar contamination was also observed for some instruments. The pyranometers located on the ship were found to be within 2% from each other at the diurnal solar peak. When compared to the buoys, we found that the WHOTS-5 was underestimating solar radiation by about 5% at maximum solar peak, while the WHOTS-6 sensors were within 2%. The reasons are probably due to salt contamination on the WHOTS-5 pyranometer domes.

The wind speed comparisons revealed that the anemometers located on top of the bridge mast were in very good agreement with the bow tower sonic in the (~ -30°, ~30°) relative wind direction range. However the portside propeller anemometer seems to read about $0.3m.s^{-1}$ higher and the AutoIMET unit located above the bridge roof read about $0.5\ m.s^{-1}$ lower. Outside the (~ -30°, ~30°) range, the wind speed differences between bridge and bow tower increase. The ship-measured winds were also found to be about 4% less than the buoy-measured winds.

Flow distortion effects were observed in the wind direction comparisons. While the bridge mast instruments agree very well with the bow sonic when the upwind flow is directly over

the bow, deviations up to ±10° could be observed in the (~ -60°, ~60°) relative wind direction range. The effects on the AutoIMET anemometer were more drastic ranging from +10° to -30° in the same window. The WHOTS-5 buoy wind direction was found to be erroneous due to some instrument issues which do not seem to impact its wind speed values. WHOTS-6 buoy wind directions seem to slightly differ between the two units when the wind is blowing from 100° east.

Tables 9 to 11 summarize the comparison analyses described above, and show the averaged differences between the different meteorological observation systems. Overall the *Kilo Moana* is a very good ship for meteorological observations, but regular maintenance and calibration are necessary to maintain the accuracy of the instruments within reasonable limits required for the SAMOS program (Fairall et al., 2007). The accuracy target estimates are presented in the table 1.7 below, with the red values indicating improvements to be made from the 2009 WHOTS-6 Field evaluation. For accurate wind speed and direction measurements, and thus better eddy covariance flux measurements, we strongly recommend the use of a bow mast in order to reduce the errors associated with flow distortion.

Parameter	Accuracy of Mean (bias)
Wind direction	3°
Wind speed	0.2 $m.s^{-1}$
Air Temperature	0.2 °C
Relative Humidity	2%
Radiation LW in	5 $W.m^{-2}$
Radiation SW in	5 $W.m^{-2}$
Sea Temperature	0.1 °C

Table 8. Accuracy targets for SAMOS

Air temperature (˚C)	PSD	W5	W6_7
KMrot	-1.13	-1.32	-1.99
KMrtd	-0.54	-0.74	-1.43
AI	0.19	-0.08	-0.74
PSD	0	-0.27	-0.93
W5	0.27	0	/
W6_7	0.93	/	0
W6_19	0.41	/	-0.52
Relative humidity (%)	PSD	W5	W6_7
KMrot	-1.05	0.99	-0.79
AI	0.92	2.84	0.87
PSD	0	1.96	0.07
W5	-1.96	0	/
W6_7	-0.07	/	0
W6_19	0	/	0.64
Sea temperature (˚C)	PSD	W5	W6_7
KM-0.25	-0.07	0	0
PSD-0.15	0	0.06	0.05
W5	-0.06	0	/
W6_7	-0.05	/	0
W6_19	-0.05	/	0

Table 9. Summary of differences for air temperature, relative humidity and sea temperature.

Shortwave radiation (W/m2)	PSD Eppley	W5	W6_7
KM	-20.81	36.83	-10.79
AI	-19.5	41.56	-1.55
PSD K&Z	-11.9	39.37	-7.97
PSD Eppley	0	38.82	2.64
W5	-38.82	0	/
W6_7	-2.64	/	0
W6_19	-16.98	/	-14.34
Longwave radiation (W/m2)	PSD Eppley	W5	W6_7
KM	1.82	0.38	0.72
AI	6.49	4.19	2.83
PSD K&Z	4.52	3.05	1.21
PSD Eppley	0	-1.82	0.06
W5	1.82	0	/
W6_7	-0.06	/	0
W6_19	1.34	/	1.4

Table 10. Summary of differences for radiation measurements.

Wind direction (deg)	PSD bow	PSD bridge	W5	W6_7
KM port	8.14/-6.56	4.96/-1.75	/	4.96/1.06
KM stbd	8.56/-2.76	5.38/2.05	/	4.86/0.47
AI	3.31/-18.21	0.13/-13.4	/	-5.38/-10.69
PSD bow	0	-3.18/4.81	/	0.23/0.12
PSD bridge	3.18/-4.81	0	/	2.66/-1.22
W5	/	/	0	/
W6_7	-0.23/-0.12	-2.66/1.22	/	0
W6_19	-1.81/-4.68	-4.24/-3.34	/	-1.58/-4.56
Wind speed (m/s)	PSD bow	PSD bridge	W5	W6_7
KM port	0.49/0.17	0.16/0.27	-0.06/-0.03	0/-0.11
KM stbd	0.38/-0.28	0.05/-0.18	-0.34/-0.23	-0.30/-0.60
AI	-0.11/-0.68	-0.44/-0.58	-0.82/-0.87	-0.82/-0.92
PSD bow	0	-0.33/0.1	-0.46/-0.27	-0.38/-0.36
PSD bridge	0.33/-0.1	0	-0.32/-0.20	-0.21/-0.26
W5	0.46/0.27	0.32/0.20	0	/
W6_7	0.38/0.36	0.21/0.26	/	0
W6_19	0.35/0.08	0.18/-0.04	/	-0.03/-0.3

Table 11. Summary of differences for wind speed and direction. Values left of '/' represent the average for the port side, while the right represent starboard averages.

References

Bradley, E.F. and Fairall, C.W. , 2007 A guide to making climate quality meteorological and flux measurements at sea. NOAA Technical Memorandum OAR PSD-311, Earth System Research Laboratory, Boulder, CO.

Fairall, C. W., E. F. Bradley, J. E. Hare, A. A. Grachev, and J. B. Edson, 2003: Bulk parameterization of air-sea fluxes: Updates and verification for the COARE algorithm. J. Climate, 16, 571-591.

Whelan, Sean P. et al., 2010: WHOI Hawaii Ocean Timeseries Station (WHOTS): WHOTS-6 2009 mooring turnaround cruise report, Woods Hole Oceanog. Inst. Tech. Report., WHOI-20-02

Moran K., S. Pezoa, C. Fairall, T. Ayers, A. Brewer, C. Williams, and S. de Szoeke, 2010: A Motion Stabilized W-band Radar for Shipboard Observations of Marine Boundary Layer Clouds, Bound.-Layer. Meteor., submitted.

Appendix A. Close-up pictures of the Kilo Moana's mast setup

Figure A 1. Top left: portside view from the KM mast (anemometer, optical raingauge). Top right: starboard view from the KM mast (anemometer, siphon raingauge, radiometers). Bottom left: close-up view of the portside optical raingauge. Bottowm right: downward close-up view on the Rotronics T/RH unit, and the RTD air temperature sensor.

Figure A 2. Left: portside back view from the KM mast (AutoIMET pressure, T/RH sensors). Right: starboard back view from the KM mast (AutoIMET radiometers, and T/RH unit).

Figure A 3. Left: Inlet tube of the KM pressure sensor. Right: Location of the pressure sensor in the aft laboratory (lab#1).